Nuclear Science and Techniques (2025) 36:199
https://doi.org/10.1007/s41365-025-01715-2

Identification of ^{3}He–^{3}H clusters in the ^{6}Li+^{89}Y experiment using particle-γ coincidence measurement

Ming-Li Wang[1] · B. Pinheiro[2] · Shi-Peng Hu[3,4] · Guang-Xin Zhang[5] · Gao-Long Zhang[1] · Huan-Qiao Zhang[6] · Hui-Bin Sun[3,4] · H. Watanabe[1] · Chun-Lei Zhang[7] · D. Testov[8,9] · P. R. John[8,9] · J. J. Valiente-Dobón[10] · A. Goasduff[8,9] · M. Siciliano[10,11,12] · F. Galtarossa[10] · F. Recchia[8,9] · D. Mengoni[8,9] · D. Bazzacco[8,9] · J. J. S. Alves[13] · J. L. Ferreira[2] · J. Lubian[2]

Received: 3 August 2024 / Revised: 19 October 2024 / Accepted: 15 November 2024 / Published online: 13 August 2025

Abstract The ^{6}Li+^{89}Y experiment was performed to explore the reaction mechanism induced by a weakly bound nucleus ^{6}Li and its cluster configuration. The particle-γ coincidence method was used to identify the different reaction channels. The γ-rays coincident with ^{3}He/^{3}H indicate that the ^{3}H/^{3}He stripping reaction plays a significant role in the formation of Zr/Nb isotopes. The obtained results support the existence of a ^{3}He–^{3}H cluster in ^{6}Li. Direct and sequential transfer reactions are adequately discussed, and the FRESCO code is used to perform precise finite-range cyclic redundancy check calculations. In the microscopic calculation, direct cluster transfer is more predominant than sequential transfer in ^{3}H transfer. However, the direct cluster transfer is of comparable magnitude to the sequential transfer in the ^{3}He transfer.

Keywords Coincidence measurement technique · Weakly bound nuclei · Direct cluster transfer · Sequential transfer · CRC calculations

1 Introduction

Nuclear clustering describes the emergence of structures in nuclear physics whose properties resemble those of atomic molecules. Atomic systems exhibit a rich phenomenology of different types of chemical bonds, complex rotational and vibrational excitations, and intricate structural

This work was supported by the National Natural Science Foundation of China under Grant Nos. U2167204, 11975040, 111 Center (B20065). Brazilian authors were supported in part by local funding agencies CNPq, FAPERJ, CAPES, and INCT-FNA (Instituto Nacional de Ciência e Tecnologia, Física Nuclear e Aplicações), Research Project No. 464898/2014-5. Marco Siciliano's work was partially supported by the US Department of Energy, Office of Science, and Office of Nuclear Physics (DE-AC02-06CH11357). S. P. Hu's work was supported by Nuclear Energy Development and Research Project No. HNKF202224(28), Ling Chuang Research Project of the China National Nuclear Corporation No. CNNC-LCKY-2023 and No. 20221024000072F6-0002-7, Guangdong Key Research and Development Program No. 2020B040420005, Guangdong Basic and Applied Basic Research Foundation No. 2021B1515120027.

✉ Shi-Peng Hu
husp@szu.edu.cn

Guang-Xin Zhang
zhanggx37@mail.sysu.edu.cn

Gao-Long Zhang
zgl@buaa.edu.cn

J. Lubian
jlubian@id.uff.br

[1] School of Physics, Beihang University, Beijing 100191, China

[2] Instituto de Física, Universidade Federal Fluminense, Niterói, Rio de Janeiro 24210-340, Brazil

[3] Institute for Advanced Study in Nuclear Energy and Safety, College of Physics and Optoelectronic Engineering, Shenzhen University, Shenzhen 518060, China

[4] Shenzhen Key Laboratory of Research and Manufacture of High Purity Germanium Materials and Detectors, Shenzhen University, Shenzhen 518060, China

[5] Sino-French Institute of Nuclear Engineering and Technology, Zhuhai 519082, China

[6] China Institute of Atomic Energy, Beijing 102413, China

geometries. The occurrence of clusters is well known in macroscopic and microscopic matter, ranging from astrophysics to nuclear physics [1]. Clustering structures emerge from a delicate balance among repulsive short-range forces, Pauli blocking effects, attractive medium-range nuclear forces, and long-range Coulomb repulsions among protons. Protons and neutrons have nearly equal masses, unlike heavy ions surrounded by electrons. Many studies have shown that nucleons tend to form clusters [2–4] such as α clusters.

The α particle is the most likely form of a cluster owing to its high symmetry and binding energy. Evidence for the presence of α clusters comes from nuclear structure calculations and measurements of α decay, such as cluster breaking effects on 3α structures in ^{12}C [4–6]. Recent theoretical studies have revealed the formation of 3α-cluster structures, which are independent of any assumptions regarding the presence of α clusters [7–11]. The experiment ^{2}H(^{16}C, ^{4}He+^{12}Be)^{2}H [12] investigated the inelastic excitation, cluster decay, and linear-chain clustering structure in neutron-rich ^{16}C. The decay paths from the ^{16}C resonances to various states and Q-value spectra of ^{16}C were measured. In addition, a large number of 4α events were recorded in an experiment on ^{12}C(^{16}O, ^{16}O)^{12}C [13]. These studies on α clusters are critical for understanding the synthesis of heavier elements in the universe [14] and other structures of bound nuclei.

The weakly bound nuclei projectiles ^{6}Li, ^{7}Li, and ^{9}Be [15–19] also exhibit α-cluster structures in the ground and resonance-excited states [20, 21]. The $\alpha + {}^{5}$He and ^{8}Be + n cluster structures have been discussed for ^{8}Be [19]. A coincidence measurement experiment was performed using a 14UD tandem accelerator at the Australian National University for ^{6,7}Li +^{208}Pb at beam energies below the fusion barrier energies [22]. The breakup modes α + α, α + t, α + d, and α + p were identified using telescope detectors. For ^{6}Li, the most intense peak in the *Q*-value spectra corresponded to the breakup of the excited states of the projectile into α and d. For ^{7}Li, the breakup into $\alpha + {}^{3}$H is prominent. The α cluster has been dominant in similar studies on particle–particle coincidence measurements [23]. Recently, the effect of the breakup on the fusion of ^{6}Li, ^{7}Li, and ^{9}Be with heavy nuclei has been discussed [15, 24]. The cross sections for incomplete fusion were found to be similar to those of the missing complete fusion, and incomplete fusion always couples with transfer channels. For example, for ^{6}Li-induced reaction by breakup-capture, Po and At nuclei can also be formed by the transfer of p, d, or α with the target. Thus, even if it is theoretically assumed (e.g., based on impact parameter considerations) [24], a distinction between transfer and breakup followed by capture is possible. Recently, the competition between transfer and incomplete has been studied [15]. In the ^{7}Li +^{209}Bi system [15], for the main incomplete fusion products, polonium isotopes, only a small fraction can be explained by projectile breakup followed by capture, where the dominant process is triton cluster transfer by combining single and coincidence measurements of light fragments. In the ^{7}Li + ^{93}Nb system [18], the triton capture mechanism has also has been observed to be dominant at about 70% when all the inclusive α-particles have been accounted for.

An exploratory experiment with radioactive beams was performed at REX-ISOLDE to test the potential of cluster-transfer reactions at the Coulomb barrier and further explore the structure of exotic neutron-rich nuclei [25, 26]. The reactions ^{7}Li(^{98}Rb, αxn) and ^{7}Li(^{98}Rb, txn) were studied using particle-γ coincidence measurements. The majority of the detected α and ^{3}H particles corresponded to ^{3}H and α transfers, whereas the percentage of ^{7}Li elastic breakup was determined to be less than 20%. The reaction mechanism has been qualitatively discussed within a distorted-wave Born approximation (DWBA) framework. Cluster-transfer reactions can be fully described as direct processes. In the early studies of the reactions ^{16}O (^{6}Li, ^{3}He) ^{19}F and ^{16}O (^{6}Li, ^{3}H) ^{19}Ne at a bombarding energy of 24 MeV, the energy spectra and angular distributions scattered ^{6}Li ions and other heavier reaction products were detected at many forward angles [27]. The results indicated that the ground-state bands of ^{19}F and ^{19}Ne are populated with a 20-fold higher intensity than other excited state bands, and the high-spin states cannot be convincing evidence for a predominantly direct reaction process. Additionally, DWBA analysis was successfully employed to establish the transfer of a three-nucleon cluster.

As mentioned earlier, the transfer reactions of ^{3}He and ^{3}H clusters on light-mass targets have been previously confirmed. However, studies on medium-mass targets are limited. In this study, cluster transfer was performed in an experiment of ^{6}Li+^{89}Y. Direct and sequential transfer reactions are discussed using cyclic redundancy check

[7] College of Nuclear Science and Technology, Beijing Normal University, Beijing 100875, China

[8] Dipartimento di Fisica, Università di Padova, 35131 Padua, Italy

[9] Istituto Nazionale di Fisica Nucleare, Sezione di Padova, Padua, Italy

[10] Laboratori Nazionali di Legnaro, INFN, 35020 Legnaro, Italy

[11] Irfu/CEA, Université de Paris-Saclay, 91190 Gif-sur-Yvette, France

[12] Physics Division, Argonne National Laboratory, Lemont, IL, USA

[13] DEFIS/ICE, Universidade Federal Rural do Rio de Janeiro, Seropédica, Rio de Janeiro 23890-000, Brazil

(CRC) calculations. The remainder of this paper is organized as follows. Section 2 presents the experimental details. Experimental results and discussion are presented in Sect. 3. The theoretical calculations are discussed in Sect. 4. Finally, conclusions are summarized in Sect. 5.

2 Experimental details

The ^{6}Li+^{89}Y experiment was performed at the Laboratori Nazionali di Legnaro, INFN, Italy. A $^{6}Li^{3+}$ beam with an average intensity of 1.0 enA was accelerated to 34 MeV using the XTU Tandem-ALPI accelerator. The ^{89}Y target, with a thickness of 550 μg/cm^2, was backed on a 340 μg/cm^2-thick ^{12}C foil to stop all the target-like reaction products. The GALILEO array, which consisted of 25 Compton-suppressed Ge detectors, was employed to collect γ-rays. The energy resolution was about 2.8 keV at 1332 keV. A 4π Si-ball detector array named EUCLIDES was used to measure light-charged particles. The EUCLIDES array comprised 40ΔE-E telescopes, where the thicknesses of ΔE and E detectors were 130 μm and 1000 μm, respectively. Detailed information on the GALILEO and EUCLIDES arrays are available in Refs. [28, 29]. A schematic of the experimental setup is shown in Fig. 1a. Because Si detectors are sensitive to radiation damage, an 200 μm-thick Al absorber was inserted between the target and EUCLIDES array to stop the elastically scattered ^{6}Li. The Al absorber shielded all the Si detectors, except for those located at angles larger than 148°. In this paper, angles larger than 148° are called uncovered angles, and the others are called covered angles. A two-dimensional correlation plot of ΔE and E detectors for the light-charged particle identification of ^{6}Li+^{89}Y at 34 MeV is shown in Fig. 1b. The proton (p), deuteron (d), tritium (^{3}H), and helium isotope particles (^{3}He and α) are clearly identified. At the covered angles, all light-charged particles were to pass through the Al absorber and ΔE detectors, whereas the particles could only pass through the ΔE detectors at the uncovered angles. The minimum energies of the particles passing through the ΔE detectors and Al absorber are listed in Table 1. Figure 1c shows the γ-rays of the main residual nuclei in a single γ spectrum detected using the GALILEO array. An analysis of the relevant γ spectrum by gating different particles (particle-γ-ray coincidence) is a viable approach for investigating their origins, as various reaction channels can generate distinct particles and residual nuclei.

3 Results and discussion

In the ^{6}Li+^{89}Y system, ^{3}H and ^{3}He evaporations are not always considered in the complete fusion reaction channel [30–32], and the breakup threshold of ^{6}Li to ^{3}He and

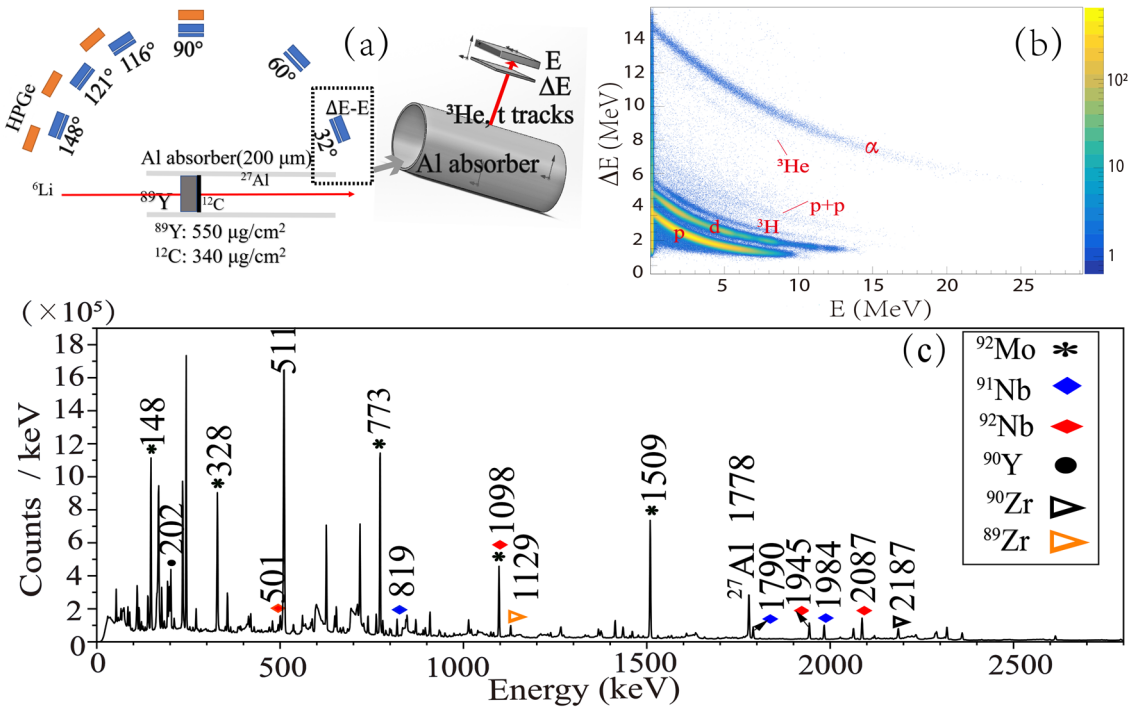

Fig. 1 (Color online) **a** Schematic of the experimental setup (sectional view); **b** two-dimensional correlation plot of ΔE and E detectors at 148° for light-charged particles identified in 34 MeV ^{6}Li+^{89}Y; **c** single γ spectrum detected by the GALILEO array

Table 1 Minimum energies of particles passing through the ΔE detectors (second column) or Al absorber and ΔE detectors (third column)

Particles	ΔE (MeV)	Al and ΔE (MeV)
^{3}H	5.710	10.56
^{3}He	13.29	23.87
α	14.88	26.89

^{3}H is as high as 15.8 MeV. The energies of the outcoming ^{3}H and ^{3}He fragments were too low to pass through the Al absorber and ΔE detectors. Therefore, ^{3}He and ^{3}H were assumed to originate from the transfer reaction.

3.1 ^{3}He $-\gamma$ coincidence

$$^{6}\mathrm{Li} + ^{89}\mathrm{Y} \rightarrow ^{92}\mathrm{Zr} + ^{3}\mathrm{He} + (-90\,\mathrm{keV}) \quad (1)$$

In Fig. 1b, ^{3}He particles can be clearly distinguished. According to the kinematics calculation for ^{3}H transfer, the energies of the outgoing ^{3}He were approximately 27 MeV, according to Eq. (1). Thus, some particles could pass through the Al absorber. The product of the reaction was ^{92}Zr, and ^{91,90}Zr could be produced by the evaporation of neutrons. ^{3}He-gated γ rays are shown in Fig. 2, where the γ-rays of ^{92,91,90}Zr are evident, and the counts of each γ ray are obtained. The normalized intensities of several significant γ rays are presented in the third and fourth columns of Table 2, with the γ-ray at 934.5 keV set to a standard reference value of 100. The direct population strengths of the excited states of ^{92}Zr are presented in Sect. 4.3. Further evidence can be obtained from ^{3}H-γ coincidence.

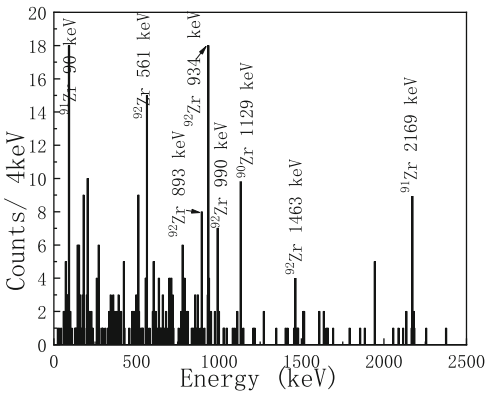

Fig. 2 (Color online) Total γ spectrum of ^{3}He $-\gamma$ coincidence over all the angles

Table 2 Relative intensities of γ-rays of ^{92}Nb normalized to the intensity of 150.0 keV γ-ray (second column) and ^{92}Zr normalized to the intensity of 934.5 keV γ-ray (fourth column) through transfer reactions

^{92}Nb of ^{3}He transfer		^{92}Zr of ^{3}H transfer	
γ-rays (keV)	Relative intensity	γ-rays (keV)	Relative intensity
123.1	26.91 ± 6.732	934.5	100 ± 26.47
148.0	100.0 ± 11.64	561.0	56.6 ± 18.50
150.0	100.0 ± 11.64	990.0	33.2 ± 15.76
194.0	86.80 ± 21.72	894.0	34.8 ± 15.26
357.5	86.53 ± 4.14	1462.0	23.5 ± 17.65
501.0	98.33 ± 13.67	–	–
711.0	89.37 ± 19.38	–	–
2087.5	61.91 ± 17.35	–	–
2287.5	136.48 ± 32.39	–	–

For ^{92}Nb, the relative intensity of 150 keV γ-ray was set to 100, and the relative intensities of other γ-rays were obtained by multiplying the relative intensity of 150 keV γ-ray after the detection efficiency correction. The same method was used for ^{92}Zr

3.2 ^{3}H$-\gamma$ coincidence

In the ^{3}H coincident γ spectrum of Fig. 3a and Fig. 4, ^{91}Nb and ^{92}Nb are the main residuals. In the inset window, the strong γ-rays 237 keV and 274 keV were the characteristic γ-rays of ^{19}Ne. The counts are significant but disappear at the uncovered angles in Fig. 3b. ^{19}Ne from the ^{3}He transfer, as shown in Eq.(2), has already been studied [27]. ^{3}H, which coincides with these γ-rays, indicates a stronger association with the transfer reaction owing to its forward trend. However, ^{16}O may originate from the support frame of the target or the backing foil. Therefore, the yield of the residues ^{19}Ne could not be obtained in this experiment.

To further analyze the main products, ^{92}Nb and ^{91}Nb, Fig. 3a shows the correlations between ^{3}H energies and different γ-rays. The projections of the energy of the γ-rays are shown on the left side, and the counts of the γ-rays of ^{91}Nb are larger when ^{3}H particles are gated. In the bottom window, the 501-keV (^{92}Nb) γ-ray-gated ^{3}H spectrum (red dots) also shows a higher energy distribution than that from 1790-keV γ rays in ^{91}Nb (blue dots). In terms of energy conservation, when the energy of the gated ^{3}H increased, the excitation energy of ^{92}Nb from ^{3}He transfer reaction decreased. Thus, fewer neutrons evaporated. The normalized intensities of certain significant γ-rays are presented in the second column of Table 2, assuming a standard intensity of 100 for the γ-rays with energy of 150 keV. According to Eq. (3), referring to the ^{3}He $-\gamma$ coincidence analysis results, ^{91}Nb and ^{92}Nb originated from ^{3}He transfer process, similar to the reaction in Ref. [27]. In the kinematics calculations, the total energy of ^{3}H was

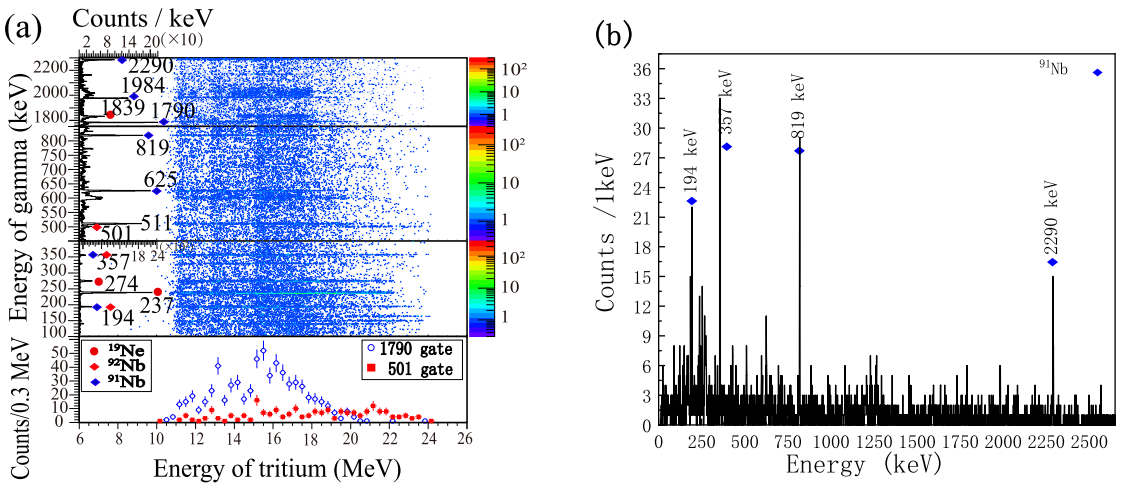

Fig. 3 (Color online) **a** Residuals at all angles on ^{3}H gating. **b** Typical γ rays of ^{3}H$-\gamma$ coincidence at uncovered angles

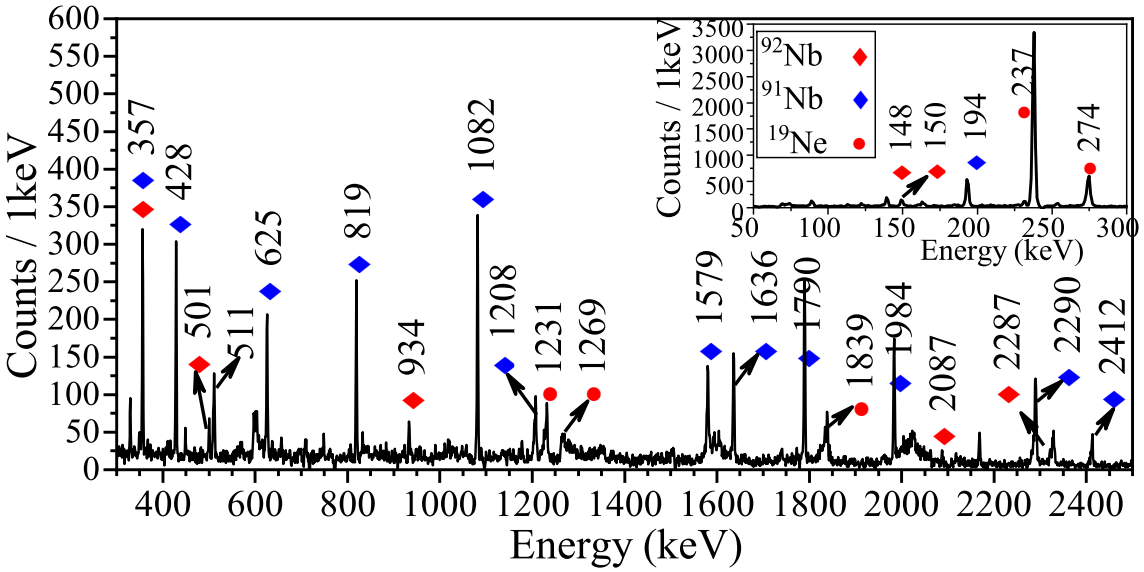

Fig. 4 (Color online) γ spectrum of ^{3}H $-$ γ coincidence at all angles

approximately 25 MeV, as shown in Eq. (3) showing that ^{3}H particles can pass through the Al absorber and be detected. ^{91}Nb, which has a neutron magic number of 50, is the one-neutron evaporation product of ^{92}Nb.

$$^{6}\mathrm{Li} + ^{16}\mathrm{O} \rightarrow ^{19}\mathrm{Ne} + ^{3}\mathrm{H} + (-7350\,\mathrm{keV}) \quad (2)$$

$$^{6}\mathrm{Li} + ^{89}\mathrm{Y} \rightarrow ^{92}\mathrm{Nb} + ^{3}\mathrm{H} + (-2120\,\mathrm{keV}) \quad (3)$$

4 Theoretical calculations for ^{3}He and ^{3}H transfers

Theoretical calculations for ^{89}Y(^{6}Li, ^{3}He)^{92}Zr and ^{89}Y(^{6}Li, ^{3}H)^{92}Nb reactions at $E_{\mathrm{lab}} = 34$ MeV were performed using exact finite-range CRC calculations with FRESCO code [33]. The São Paulo double-folding potential was used as the optical potential for both real and imaginary parts [34]. To consider channels that are not explicitly included in the entrance partition, such as breakups, we set the strength factor of the imaginary part to 0.60 [35]. The strength factor of the imaginary part was set to 0.78 for the outgoing partitions, as no couplings were considered [36]. Woods–Saxon potentials were used to build the single-particle and cluster wave functions. The diffusivity and radii were fixed at 0.65 fm and 1.25 fm, respectively, and the depth was varied to reproduce the experimental binding energy.

These transfer reactions occur in two ways: (i) Directly, where nucleons are transferred together simultaneously as a cluster, i.e., considering the cluster as a structure-less particle. (ii) Sequentially, in which the nucleons are

transferred in two or more steps, passing through intermediate partitions. Therefore, both direct and sequential processes were considered in the transfer calculations. In contrast, cross sections were obtained for two types of transfer reactions considering two different schemes: (a) SA = 1.0, which implies that the spectroscopic amplitude was set to 1.0, and (b) microscopic spectroscopic amplitudes calculated using the shell model [37].

Many theoretical studies have attempted to derive the cluster spectroscopic amplitudes, particularly for alpha particles (e.g., Refs. [38–49]). Most of these studies have used different theoretical approaches, including shell, dynamic molecular, and pure cluster models to determine the contribution of the alpha cluster to the wave function of the bound or resonant states. Others were concerned with cluster preformation for alpha emissions. In some studies, the authors claimed that the shell model failed to derive the spectroscopic properties of the states.

To verify the validity of the shell model for calculating the spectroscopic amplitudes, we compared its results with those obtained in Ref. [50] using the semi-microscopic algebraic cluster model for the $\langle {}^{16}\mathrm{O}|{}^{12}\mathrm{C}\rangle$ overlaps required in alpha transfer calculations for the $^{16}\mathrm{O}(^{12}\mathrm{C},^{16}\mathrm{O})^{12}\mathrm{C}$ reaction. We obtained results similar to those reported in Table 3 of Ref. [50]. This is confident evidence of the validity of the shell model as a reasonable approximation for deriving the spectroscopic amplitudes for cluster transfer in this study.

4.1 Calculation results of direct transfer reactions

One of the most common methods for two-particle transfer calculations is to set the spectroscopic amplitude equal to 1.0 (SA = 1.0) [51]. In this case, the nucleon spins are considered antiparallel, and $n = 1$ and $l = 0$ are assumed as the internal state of the cluster quantum number. In our case, where the cluster is composed of three nucleons, the spin of the transferred cluster is assumed to be equal to the spin of the free nucleus in its ground state. The relevant parameters for defining the cluster wave function are the principal quantum number N and the orbital angular momentum L relative to the core. N and L can be determined from the conservation of the total number of quanta in the transformation of the wave function of three independent nucleons into a cluster [52].

$$\sum_{i=1}^{3} 2(n_i - 1) + l_i = 2(N - 1) + L + 2(n - 1) + l, \qquad (4)$$

where n_i and l_i $(i = 1, \ldots, 3)$ are the quantum numbers of each nucleon. For ^{3}He and ^{3}H clusters, $l = 1$ because the unpaired particle is in the $1p_{3/2}$ orbital. In addition, the spectroscopic amplitudes for the overlaps of the wave functions for both the projectile and target are set to 1.0. However, these spectroscopic amplitudes might be unrealistic. The nuclear structures of the projectile, target, and residuals are ignored.

The level scheme of the nuclei and couplings adopted in the direct transfer calculations is shown in Fig. 5 for both transfer reactions. Here, we are interested in the order of magnitude rather than in a quantitative description of the reaction process. Because the selection rules for the transfer of particles are relevant in these processes, for each case, the states are characterized by the spin, parity, and energy values considered in the calculations according to the total angular momentum J, orbital momentum L, and spin of the transferred cluster. The theoretical results of the direct ^{3}H and ^{3}He transfers for SA = 1.0 are shown in Tables 3 and 4, respectively. The transfer cross sections are of the order of mb. However, these results are overestimated because of unrealistic spectroscopic amplitudes.

The next step was to calculate realistic spectroscopic amplitudes for the projectile and target overlap. Microscopic spectroscopic amplitudes calculated from the shell model were necessary to obtain these spectroscopic amplitudes. These were obtained by performing shell model calculations using the NuShellX code [53]. For the target overlaps, a closed ^{78}Ni core and valence protons in the $1f_{5/2}$, $2p_{3/2}$, $2p_{1/2}$, and $1g_{9/2}$ orbitals and valence neutrons in the $1g_{7/2}$, $2d_{5/2}$, $2d_{3/2}$, $3s_{1/2}$, and $1h_{11/2}$ orbitals were considered. Because of computational limitations, certain restrictions were imposed on the valence proton orbitals. Specifically, within the $1g_{9/2}$ orbit, we determined that a maximum of six protons could occupy this orbital. The n − n, p − p, and n − p effective phenomenological interactions were based on *jj*45*apn* interaction [54], in which the two-body matrix elements were determined considering the charge-dependent Bonn potential (CD-Bonn) [55, 56]. In this interaction, the single-particle energies for proton model space were set to $\epsilon_{1f_{5/2}} = -0.7166\,\mathrm{MeV}$, $\epsilon_{2p_{3/2}} = 1.1184\,\mathrm{MeV}$, $\epsilon_{2p_{1/2}} = 1.1262\,\mathrm{MeV}$, and $\epsilon_{1g_{9/2}} = 0.1785\,\mathrm{MeV}$. In addition, the single-particle energies for the neutron space were set to $\epsilon_{1g_{7/2}} = 5.7402\,\mathrm{MeV}$, $\epsilon_{2d_{5/2}} = 2.4422\,\mathrm{MeV}$, $\epsilon_{2d_{3/2}} = 2.5148$ MeV, $\epsilon_{3s_{1/2}} = 2.1738\,\mathrm{MeV}$, and $\epsilon_{1h_{11/2}} = 2.6795\,\mathrm{MeV}$. In our approach, we modified the single-particle energies for the proton model space, for which the values were obtained from the *glbepn* interaction [57]. In this context, $\epsilon_{1f_{5/2}} = -3.706\,\mathrm{MeV}$, $\epsilon_{2p_{3/2}} = -2.133\,\mathrm{MeV}$, $\epsilon_{2p_{1/2}} = -1.101\,\mathrm{MeV}$, and $\epsilon_{1g_{9/2}} = -0.638\,\mathrm{MeV}$ were considered. With this modification, the spectra of the ^{89}Y, ^{92}Zr, and ^{92}Nb nuclei could be described quite well. In addition, we built an effective phenomenological interaction that could describe the single-particle energies of ^{89}Y, ^{92}Zr, and ^{92}Nb

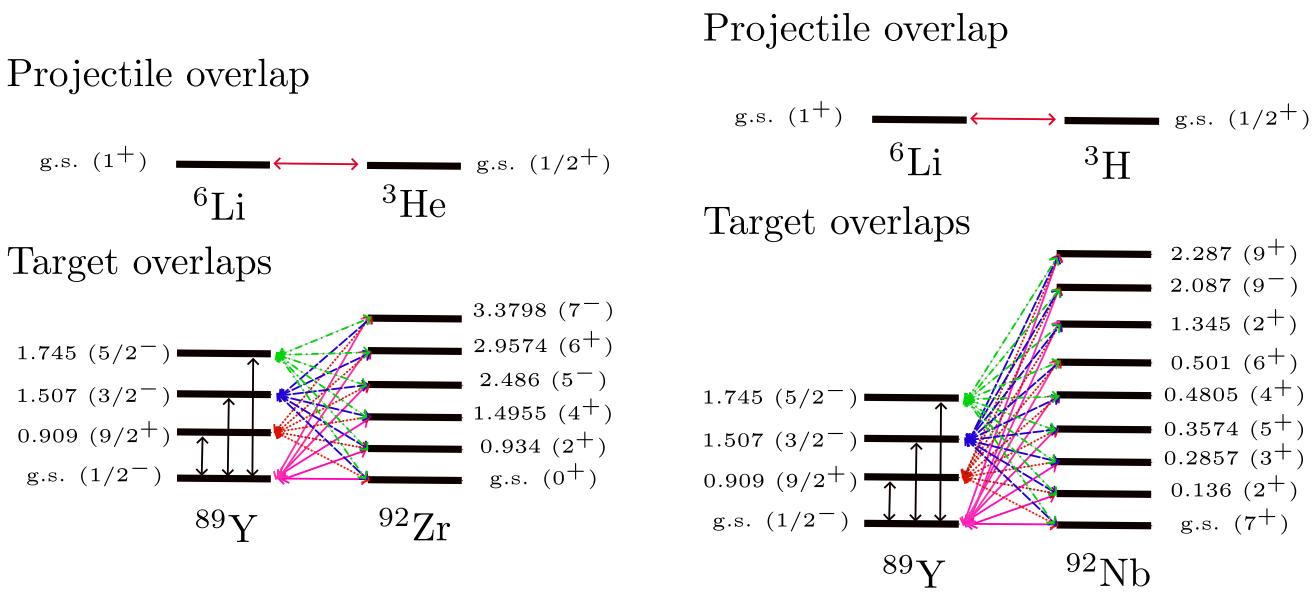

Fig. 5 (Color online) Coupling scheme considered for the projectile and target overlaps in both direct reactions. The energies are given in MeV. **a** Coupling scheme considered in the ^{89}Y (^{6}Li, ^{3}He) ^{92}Zr reaction. **b** Coupling scheme considered in the ^{89}Y (^{6}Li, ^{3}H) ^{92}Nb reaction

Table 3 For direct ^{3}H transfer and sequential ^{3}H transfer: States involved in the CRC calculations for the ^{89}Y(^{6}Li,^{3}He)^{92}Zr reaction

Outgoing channel		Integrated cross section (mb)			
^{3}He $J^{\pi}E$ (keV)	^{92}Zr	Direct (SA = 1.0)	Direct (microscopic calculations)	Sequential (SA = 1.0)	Sequential (microscopic calculations)
$1/2^{-}$ 0.0	0^{+} 0.0	0.9121	2.302×10^{-4}	6.623×10^{-3}	1.168×10^{-7}
	2^{+} 934.5	4.948	2.381×10^{-5}	1.726×10^{-2}	6.756×10^{-7}
	4^{+} 1495.5	8.556	3.884×10^{-5}	5.461×10^{-2}	3.282×10^{-7}
	5^{-} 2486.0	13.28	2.642×10^{-5}	9.843×10^{-3}	3.321×10^{-9}
	6^{+} 2957.4	11.78	3.543×10^{-6}	4.238×10^{-2}	7.295×10^{-7}
	7^{-} 3379.0	9.985	1.170×10^{-5}	1.143×10^{-2}	8.325×10^{-6}

Integrated transfer cross sections for both direct and sequential transfers considering couplings between ^{89}Y and ^{92}Zr states are shown

nuclei. This new interaction was based on *jj*45*pna* and *glbepn* interactions [54]. For the projectile overlap, $1s_{1/2}$, $1p_{3/2}$, and $1p_{1/2}$ were considered for both the neutron and proton model spaces for which a no-core interaction was used [58]. Single-particle energies and two-body matrix elements were inspired by the Warburton and Brown interactions [59]. The theoretical results for the direct ^{3}H and ^{3}He transfers are shown in Tables 3 and 4, respectively.

We observed that the integrated transfer cross sections of both reactions decreased when microscopic spectroscopic amplitudes were used. These results were expected because this cluster configuration should have a low probability in these nuclei. The calculated spectroscopic amplitudes are presented in the Appendixes.

4.2 Calculation of sequential transfer reactions

The calculations also considered sequential processes in which the three nucleons are transferred. We performed calculations for multi-step transfer reactions passing through the intermediate partitions. We focused on two two-step sequential transfers, ^{2}H + n and ^{2}H + p because these are the only reactions that pass through partitions with stable projectile-like nuclei. The others occur through unstable nuclei (^{5}Li or ^{5}He), which is unlikely because they are two-step processes and the unbound particles decay easily. Nevertheless, some tests that included ground states as bounds were also performed. The cross sections were observed to be very small. The cross sections for these transfer reactions were three orders of magnitude lower than those for direct cluster transfer. Therefore, we do not

Table 4 For direct ^{3}He transfer and sequential ^{3}He transfer: States involved in the CRC calculations for the ^{89}Y (^{6}Li, ^{3}H) ^{92}Nb reaction

Outgoing channel		Integrated cross section (mb)			
^{3}H $J^{\pi}E$ (keV)	^{92}Nb	Direct (SA = 1.0)	Direct (microscopic calculations)	Sequential (SA = 1.0)	Sequential (microscopic calculations)
$1/2^{-}$ 0.0	7^{+} 0.0	5.611	4.397×10^{-6}	4.580×10^{-4}	1.284×10^{-5}
	2^{+} 136.0	2.347	1.415×10^{-6}	3.523×10^{-3}	1.850×10^{-5}
	3^{+} 285.7	2.670	1.081×10^{-6}	3.542×10^{-3}	4.497×10^{-6}
	5^{+} 357.4	7.913	5.189×10^{-6}	4.979×10^{-3}	9.804×10^{-6}
	4^{+} 480.5	7.495	3.835×10^{-6}	5.640×10^{-3}	7.630×10^{-6}
	6^{+} 501.0	8.059	4.510×10^{-6}	4.053×10^{-3}	4.276×10^{-6}
	2^{+} 1345.5	5.253	3.968×10^{-8}	4.149×10^{-3}	2.159×10^{-7}
	9^{-} 2087.5	7.229	5.352×10^{-7}	–	–
	9^{+} 2287.2	4.278	7.684×10^{-8}	–	–

Integrated transfer cross sections for both direct and sequential transfers, respectively, considering couplings between ^{89}Y and ^{92}Nb states are shown

provide details here and consider only two two-step sequential transfer reactions passing through the same intermediate partition (^{4}He + ^{91}Zr). Three excited and ground states were considered for ^{91}Zr, as shown in Appendix C. These reactions involve only stable nuclei or nuclei with long half-lives. In these two transfer reactions, either a proton is transferred after a ^{2}H-like (a correlated n-p) for the ^{3}He sequential transfer reaction, or a neutron is transferred after a ^{2}H-like (a correlated n-p) for the ^{3}H sequential transfer reaction. Similarly, the São Paulo potential (SPP) was used for the real and imaginary parts of the optical potential. As no couplings were considered in the intermediate partitions, the strength factor of the imaginary part was set to 0.78, as in the outgoing partitions. The Woods–Saxon potential was used to build single-particle wave functions, in which the parameters were varied to reproduce the corresponding experimental binding energies. The ^{91}Zr states used in the theoretical calculations were obtained according to Brink's criteria for optimal excitation energies [60]. The spectroscopic amplitude results are presented in the Appendix C.

The level scheme and the couplings adopted in the sequential transfer calculations are shown in Fig. 6 for both the reactions. Theoretical calculations were performed considering SA = 1.0 for the ^{2}H transfer (in the first step), and spectroscopic amplitudes were set equal to 1.0 for proton and neutron transfer (in the second step). The results are summarized in Tables 3 and 4. Comparing the results shown in Tables 3 and 4, we observed that the cross sections of the direct process were three orders of magnitude larger than those of the sequential process; therefore, the sequential process is negligible compared to the direct process.

The microscopic spectroscopic amplitudes calculated from the shell model are shown in a sequential process. The same interaction and model space were used to evaluate the microscopic spectroscopic amplitudes that were used in the direct reaction calculations above. In the first step, a deuterium-like particle was transferred, followed by a proton or neutron when microscopic spectroscopic amplitudes were used. In this case, the independent coordinate model was used [51] in which the coordinates of the nucleons are transformed to the relative coordinates between the neutron and proton and that of its center of mass relative to the α core. The spectroscopic amplitudes were calculated for the correlated n-p, including the projectile-like and target-like overlaps. In the second step, a neutron was transferred to the ^{3} H-stripping reaction. Similarly, a proton was transferred in the second step of ^{3}He transfer.

The theoretical results for the sequential transfer reactions with microscopic spectroscopic amplitudes are presented in Tables 3 and 4. The integrated transfer cross sections of the 9^{-} and 9^{+} states for ^{92}Nb are missing. This is because the selection rules prohibit these transitions during the sequential transfer process in the used model space. Comparing the results in Table 3, we can conclude that the sequential process is negligible for most of the studied states when microscopic spectroscopic amplitudes are applied to the ^{3}H transfer reaction. Conversely, sequential transfer is relevant to the ^{3}He transfer reaction when compared with the direct transfer process, as they have cross sections of the same order of magnitude.

These results can be explained by examining the structures of the residual nuclei. The transfer cross section is proportional to the spectroscopic amplitudes of two

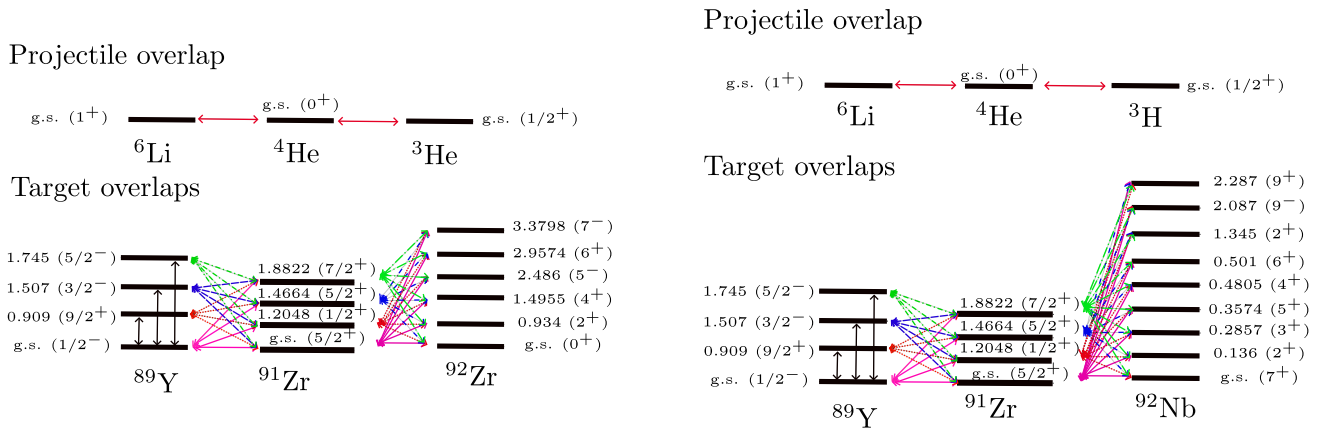

Fig. 6 (Color online) Coupling scheme considered for the projectile and target overlaps for sequential process. The energies are given in MeV. **a** Coupling scheme considered in the ^{89}Y (^{6}Li, ^{3}He) ^{92}Zr reaction. **b** Coupling scheme considered in the ^{89}Y (^{6}Li, ^{3}H) ^{92}Nb reaction

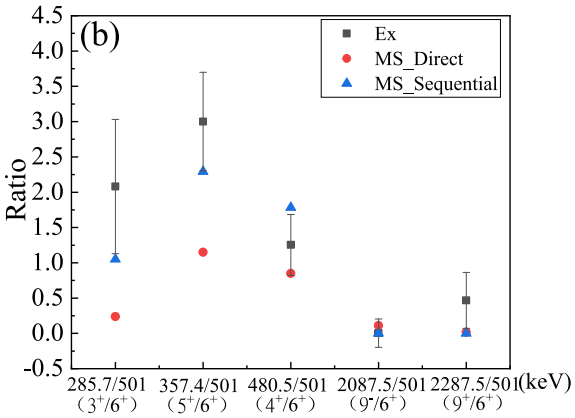

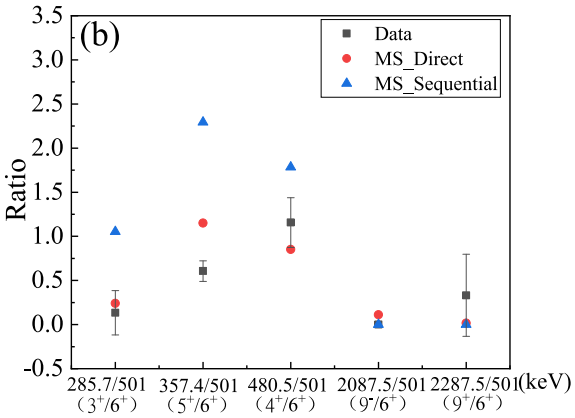

Fig. 7 (Color online) **a** Ratio of cross sections of different excited states of ^{92}Zr to that of the first excited state (2^{+}) observed in experiment. **b** Ratio of cross sections of different excited states of ^{92}Nb to that of the state (501-keV 2^{+}) observed in the experiment. The MS_Direct means the theoretical results of direct transfer reaction using microscopic spectroscopic amplitudes calculated from shell model, and MS_Sequential represents sequential transfer reaction; data indicate the experimental data

overlaps: one for the projectile and the second for the target. The projectile overlaps are similar because the transferred neutrons or protons in the second step lie on the same shell. The protons and neutrons transferred to the target-like nucleus (^{91}Zr) will occupy different orbitals in the residual nuclei. Therefore, the spectroscopic amplitudes of the second step are very different, and consequently, the two-step transfer is very different in the ^{2}H + n and ^{2}H + p transfers.

4.3 Comparison with experimental data

The interplay between direct and sequential transfer reactions is discussed in Ref. [61] for deuteron transfer. The relevance of both processes in our experimental data is also discussed. The intensities of some γ-rays are listed in Table 2. Therefore, the relative ratios of some states that are directly populated can be defined to compare the theoretical results in the framework of microscopic spectroscopic amplitude calculations with the experimental data. The 6^{+} state of ^{92}Nb was used as a benchmark, whereas the 2^{+} state was used for ^{92}Zr. The selected states were guided by the fact that they decayed only to the ground state. The results are presented in Fig. 7. Figure 7a shows the ratio of the cross sections of the different excited states of ^{92}Zr to that of the first excited state (2^{+}) observed experimentally. The experimental and theoretical ratios for 6^{+} and 7^{-} states were in good agreement for direct transfer. The theoretical and experimental ratios for the other two states were also of the same order of magnitude for the direct ^{3}H transfer reaction. The sequential transfer cross sections were in good agreement with the experimental ratios for the three lower energy states. As mentioned previously, by comparing the results presented in Table 4, the sequential and direct processes were of the same order of magnitude in the ^{3}He transfer reactions. Therefore, both

processes are relevant when microscopic spectroscopic amplitudes are used. The ratios of most states are consistent with the theoretical calculations, as shown in Fig. 7b. For ^{92}Nb, the errors of states 285.7 keV(3^+) and 357.4 keV(5^+) were larger, because the γ-rays 357.4 keV and 194.8 keV also emanate from ^{91}Nb.

5 Conclusion

In this study, the transfer reactions of ^{3}He and ^{3}H by charged particles and γ-ray coincidence. From the $^3\mathrm{He}-\gamma$ coincident measurement, one ^{3}H-stripping reaction contributed to the formation of Zr isotopes and provided evidence for the ^{3}He transfer reaction by ^{3}H-γ coincident measurements. In the coincident results of ^{3}H-γ, two types of transfer reaction products were obtained: ^{19}Ne from the reaction with ^{16}O and ^{92}Nb from the reaction with the target nucleus ^{89}Y. CRC calculations and comparison of the relative cross sections of different excited states observed in the experiment confirmed the existence of ^{3}He and ^{3}H clusters in ^{6}Li. However, more experiments are required because of the limitations of the experimental statistics.

Appendix A: Spectroscopic amplitudes for $<^{89}\mathrm{Y}|^{92}\mathrm{Nb}>$ overlaps, in the ^{3}He cluster transfer

See Table 5.

Table 5 ^{3}He-spectroscopic amplitudes for the target overlaps used in CRC calculation, where N, L, and J are the principal quantum number, orbital angular momentum, and total angular momentum of the ^{3}He cluster, respectively

Initial state	N	L	J	Final state	S.A.
$^{89}\mathrm{Y}_{g.s.}(1/2^-)$	3	7	13/2	$^{92}\mathrm{Nb}_{\mathrm{g.s.}}(7^+)$	− 0.00139
	3	7	15/2	$^{92}\mathrm{Nb}_{\mathrm{g.s.}}(7^+)$	− 0.00780
	6	1	3/2	$^{92}\mathrm{Nb}_{0.136}(2^+)$	− 0.00010
	5	3	5/2	$^{92}\mathrm{Nb}_{0.136}(2^+)$	0.00402
	4	5	9/2	$^{92}\mathrm{Nb}_{0.358}(5^+)$	0.00129
	4	5	11/2	$^{92}\mathrm{Nb}_{0.358}(5^+)$	0.00562
	5	3	7/2	$^{92}\mathrm{Nb}_{0.481}(4^+)$	0.00126
	4	5	9/2	$^{92}\mathrm{Nb}_{0.481}(4^+)$	− 0.00555
	4	5	11/2	$^{92}\mathrm{Nb}_{0.501}(6^+)$	0.00129
	3	7	13/2	$^{92}\mathrm{Nb}_{0.501}(6^+)$	− 0.00853
	6	1	3/2	$^{92}\mathrm{Nb}_{1.346}(2^+)$	− 0.00026
	5	3	5/2	$^{92}\mathrm{Nb}_{1.346}(2^+)$	− 0.00014
	3	8	17/2	$^{92}\mathrm{Nb}_{2.088}(9^-)$	0.00034
	2	10	19/2	$^{92}\mathrm{Nb}_{2.088}(9^-)$	− 0.00441
	2	9	17/2	$^{92}\mathrm{Nb}_{2.287}(9^+)$	− 0.00021
	2	9	19/2	$^{92}\mathrm{Nb}_{2.287}(9^+)$	0.00024
	3	9	17/2	$^{92}\mathrm{Nb}_{2.287}(9^+)$	0.00036
$^{89}\mathrm{Y}_{0.909}(9/2^+)$	4	4	7/2	$^{92}\mathrm{Nb}_{\mathrm{g.s.}}(7^+)$	0.00158
	4	4	9/2	$^{92}\mathrm{Nb}_{\mathrm{g.s.}}(7^+)$	0.00159
	3	6	11/2	$^{92}\mathrm{Nb}_{\mathrm{g.s.}}(7^+)$	− 0.00019
	4	6	11/2	$^{92}\mathrm{Nb}_{\mathrm{g.s.}}(7^+)$	− 0.00033
	3	6	13/2	$^{92}\mathrm{Nb}_{\mathrm{g.s.}}(7^+)$	− 0.00013
	4	6	13/2	$^{92}\mathrm{Nb}_{\mathrm{g.s.}}(7^+)$	− 0.00038
	3	8	15/2	$^{92}\mathrm{Nb}_{\mathrm{g.s.}}(7^+)$	0.00033
	3	8	17/2	$^{92}\mathrm{Nb}_{\mathrm{g.s.}}(7^+)$	0.00061
	2	10	19/2	$^{92}\mathrm{Nb}_{\mathrm{g.s.}}(7^+)$	− 0.00028
	2	10	21/2	$^{92}\mathrm{Nb}_{\mathrm{g.s.}}(7^+)$	− 0.00117
	1	12	23/2	$^{92}\mathrm{Nb}_{\mathrm{g.s.}}(7^+)$	0.00007
	5	2	5/2	$^{92}\mathrm{Nb}_{0.136}(2^+)$	0.00953
	4	4	7/2	$^{92}\mathrm{Nb}_{0.136}(2^+)$	− 0.00036
	5	4	7/2	$^{92}\mathrm{Nb}_{0.136}(2^+)$	− 0.00038
	4	4	9/2	$^{92}\mathrm{Nb}_{0.136}(2^+)$	0.00038
	5	4	9/2	$^{92}\mathrm{Nb}_{0.136}(2^+)$	0.00034
	3	6	11/2	$^{92}\mathrm{Nb}_{0.1366}(2^+)$	0.00009
	4	6	11/2	$^{92}\mathrm{Nb}_{0.136}(2^+)$	0.00054
	4	6	13/2	$^{92}\mathrm{Nb}_{0.136}(2^+)$	− 0.00016
	6	0	1/2	$^{92}\mathrm{Nb}_{0.358}(5^+)$	− 0.01160
	5	2	3/2	$^{92}\mathrm{Nb}_{0.358}(5^+)$	0.00187
	5	2	5/2	$^{92}\mathrm{Nb}_{0.358}(5^+)$	0.01450
	4	4	7/2	$^{92}\mathrm{Nb}_{0.358}(5^+)$	0.00100
	4	4	9/2	$^{92}\mathrm{Nb}_{0.358}(5^+)$	0.00138
	4	6	11/2	$^{92}\mathrm{Nb}_{0.358}(5^+)$	0.00012
	3	6	13/2	$^{92}\mathrm{Nb}_{0.358}(5^+)$	0.00010

Table 5 continued

Initial state	N	L	J	Final state	S.A.
	4	6	13/2	$^{92}Nb_{0.358}(5^+)$	− 0.00041
	3	8	15/2	$^{92}Nb_{0.358}(5^+)$	− 0.00007
	3	8	17/2	$^{92}Nb_{0.358}(5^+)$	0.00059
	2	10	19/2	$^{92}Nb_{0.358}(5^+)$	0.00066
$^{89}Y_{0.909}(9/2^+)$	6	0	1/2	$^{92}Nb_{0.481}(4^+)$	− 0.00655
	5	2	3/2	$^{92}Nb_{0.481}(4^+)$	− 0.00108
	5	2	5/2	$^{92}Nb_{0.481}(4^+)$	0.01370
	4	4	7/2	$^{92}Nb_{0.481}(4^+)$	− 0.00111
	4	4	9/2	$^{92}Nb_{0.481}(4^+)$	0.00106
	3	6	11/2	$^{92}Nb_{0.481}(4^+)$	0.00015
	4	6	11/2	$^{92}Nb_{0.481}(4^+)$	0.00051
	3	6	13/2	$^{92}Nb_{0.481}(4^+)$	− 0.00007
	4	6	13/2	$^{92}Nb_{0.481}(4^+)$	− 0.00014
	3	8	15/2	$^{92}Nb_{0.481}(4^+)$	− 0.00061
	3	8	17/2	$^{92}Nb_{0.481}(4^+)$	0.00041
	5	2	3/2	$^{92}Nb_{0.501}(6^+)$	0.00014
	6	2	3/2	$^{92}Nb_{0.501}(6^+)$	− 0.00021
	6	2	5/2	$^{92}Nb_{0.501}(6^+)$	− 0.00177
	4	4	7/2	$^{92}Nb_{0.501}(6^+)$	− 0.00040
	5	4	7/2	$^{92}Nb_{0.501}(6^+)$	0.00028
	4	4	9/2	$^{92}Nb_{0.501}(6^+)$	− 0.00156
	4	6	11/2	$^{92}Nb_{0.501}(6^+)$	0.00033
	3	6	13/2	$^{92}Nb_{0.501}(6^+)$	0.00013
	3	8	15/2	$^{92}Nb_{0.501}(6^+)$	0.00048
	3	8	17/2	$^{92}Nb_{0.501}(6^+)$	− 0.00017
	2	10	19/2	$^{92}Nb_{0.501}(6^+)$	− 0.00085
	2	10	21/2	$^{92}Nb_{0.501}(6^+)$	0.00043
	5	2	5/2	$^{92}Nb_{1.346}(2^+)$	0.00050
	6	2	5/2	$^{92}Nb_{1.346}(2^+)$	0.00080
	4	4	7/2	$^{92}Nb_{1.346}(2^+)$	0.00187
	5	4	7/2	$^{92}Nb_{1.346}(2^+)$	0.00028
	4	4	9/2	$^{92}Nb_{1.346}(2^+)$	0.00096
	5	4	9/2	$^{92}Nb_{1.346}(2^+)$	0.00105
	3	6	11/2	$^{92}Nb_{1.346}(2^+)$	0.00051
	4	6		$^{92}Nb_{1.346}(2^+)$	0.00156

Table 5 continued

Initial state	N	L	J	Final state	S.A.
			11/2		
	4	6	13/2	$^{92}Nb_{1.346}(2^+)$	0.00013
	4	5	9/2	$^{92}Nb_{2.088}(9^-)$	− 0.00108
	4	5	11/2	$^{92}Nb_{2.088}(9^-)$	− 0.00530
	3	7	13/2	$^{92}Nb_{2.088}(9^-)$	− 0.00014
	3	7	15/2	$^{92}Nb_{2.088}(9^-)$	− 0.00107
	2	9	17/2	$^{92}Nb_{2.088}(9^-)$	− 0.00006
	3	9	17/2	$^{92}Nb_{2.088}(9^-)$	− 0.00004
	2	9	19/2	$^{92}Nb_{2.088}(9^-)$	− 0.00002
	3	9	19/2	$^{92}Nb_{2.088}(9^-)$	0.00002
	2	11	21/2	$^{92}Nb_{2.088}(9^-)$	0.00010
	2	11	23/2	$^{92}Nb_{2.088}(9^-)$	− 0.00013
	1	13	25/2	$^{92}Nb_{2.088}(9^-)$	− 0.00062
	1	13	27/2	$^{92}Nb_{2.088}(9^-)$	0.00117
	4	4	9/2	$^{92}Nb_{2.287}(9^+)$	0.00093
	5	4	9/2	$^{92}Nb_{2.287}(9^+)$	0.00051
	4	4	11/2	$^{92}Nb_{2.287}(9^+)$	0.00016
	5	4	11/2	$^{92}Nb_{2.287}(9^+)$	0.00099
	3	6	13/2	$^{92}Nb_{2.287}(9^+)$	0.00010
	4	6	13/2	$^{92}Nb_{2.287}(9^+)$	0.00096
	3	8	15/2	$^{92}Nb_{2.287}(9^+)$	− 0.00101
	3	8	17/2	$^{92}Nb_{2.287}(9^+)$	− 0.00116
	2	10	19/2	$^{92}Nb_{2.287}(9^+)$	0.00125
	2	10	21/2	$^{92}Nb_{2.287}(9^+)$	− 0.00188
	1	12	23/2	$^{92}Nb_{2.287}(9^+)$	0.00036
	1	12	25/2	$^{92}Nb_{2.287}(9^+)$	− 0.00034
$^{89}Y_{1.507}(3/2^-)$	4	5	11/2	$^{92}Nb_{g.s.}(7^+)$	0.00590
	3	7	13/2	$^{92}Nb_{g.s.}(7^+)$	− 0.00189
	3	7	15/2	$^{92}Nb_{g.s.}(7^+)$	− 0.00538

Table 5 continued

Initial state	N	L	J	Final state	S.A.
	2	9	17/2	$^{92}Nb_{g.s.}(7^+)$	− 0.00003
	3	9	17/2	$^{92}Nb_{g.s.}(7^+)$	0.00007
	6	1	1/2	$^{92}Nb_{0.136}(2^+)$	− 0.00495
	6	1	3/2	$^{92}Nb_{0.136}(2^+)$	0.00272
	5	3	5/2	$^{92}Nb_{0.136}(2^+)$	0.00329
	5	3	7/2	$^{92}Nb_{0.136}(2^+)$	− 0.00145
	5	3	7/2	$^{92}Nb_{0.358}(5^+)$	− 0.00470
	4	5	9/2	$^{92}Nb_{0.358}(5^+)$	− 0.00075
	4	5	11/2	$^{92}Nb_{0.358}(5^+)$	0.00371
	3	7	13/2	$^{92}Nb_{0.358}(5^+)$	0.00212
	5	3	5/2	$^{92}Nb_{0.481}(4^+)$	0.00498
	5	3	7/2	$^{92}Nb_{0.481}(4^+)$	− 0.00068
	4	5	9/2	$^{92}Nb_{0.481}(4^+)$	− 0.00408
	4	5	11/2	$^{92}Nb_{0.481}(4^+)$	0.00162
	4	5	9/2	$^{92}Nb_{0.501}(6^+)$	0.00602
	4	5	11/2	$^{92}Nb_{0.501}(6^+)$	− 0.00048
	3	7	13/2	$^{92}Nb_{0.501}(6^+)$	− 0.00560
	3	7	15/2	$^{92}Nb_{0.501}(6^+)$	0.00147
	6	1	1/2	$^{92}Nb_{1.346}(2^+)$	− 0.00099
	6	1	3/2	$^{92}Nb_{1.346}(2^+)$	0.00032
	5	3	5/2	$^{92}Nb_{1.346}(2^+)$	0.00048
	5	3	7/2	$^{92}Nb_{1.346}(2^+)$	− 0.00057
	3	8	15/2	$^{92}Nb_{2.088}(9^-)$	− 0.00215
	3	8	17/2	$^{92}Nb_{2.088}(9^-)$	− 0.00076
	2	10	19/2	$^{92}Nb_{2.088}(9^-)$	− 0.00242
	2	10	21/2	$^{92}Nb_{2.088}(9^-)$	0.00311
	3	7	15/2	$^{92}Nb_{2.287}(9^+)$	0.00027
	2	9	17/2	$^{92}Nb_{2.287}(9^+)$	− 0.00001
	3	9	17/2	$^{92}Nb_{2.287}(9^+)$	− 0.00009
	3	9	19/2	$^{92}Nb_{2.287}(9^+)$	− 0.00022
	2	11	21/2	$^{92}Nb_{2.287}(9^+)$	0.00016
$^{89}Y_{1.745}(5/2^-)$	4	5	9/2	$^{92}Nb_{g.s.}(7^+)$	0.00066
	4	5	11/2	$^{92}Nb_{g.s.}(7^+)$	0.00146
	3	7	13/2	$^{92}Nb_{g.s.}(7^+)$	− 0.00178
	3	7	15/2	$^{92}Nb_{g.s.}(7^+)$	− 0.00342
	2	9	17/2	$^{92}Nb_{g.s.}(7^+)$	− 0.00407
	2	9	19/2	$^{92}Nb_{g.s.}(7^+)$	0.01162
	6	1	1/2	$^{92}Nb_{1.346}(2^+)$	− 0.00056
	6	1	3/2	$^{92}Nb_{1.346}(2^+)$	0.00064
	5	3	5/2	$^{92}Nb_{1.346}(2^+)$	0.00147
	5	3	7/2	$^{92}Nb_{1.346}(2^+)$	− 0.00101
	4	5	9/2	$^{92}Nb_{1.346}(2^+)$	− 0.00364
	5	3	5/2	$^{92}Nb_{0.358}(5^+)$	− 0.00073
	5	3	7/2	$^{92}Nb_{0.358}(5^+)$	− 0.00111
	4	5	9/2	$^{92}Nb_{0.358}(5^+)$	0.00065
	4	5	11/2	$^{92}Nb_{0.358}(5^+)$	0.00227
	3	7	13/2	$^{92}Nb_{0.358}(5^+)$	− 0.00075
	3	7	13/2	$^{92}Nb_{0.358}(5^+)$	− 0.00603
	5	1	3/2	$^{92}Nb_{0.481}(4^+)$	− 0.00080
	5	3	5/2	$^{92}Nb_{0.481}(4^+)$	0.00105
	5	3	7/2	$^{92}Nb_{0.481}(4^+)$	0.00047
	4	5	9/2	$^{92}Nb_{0.481}(4^+)$	− 0.00227
	4	5	11/2	$^{92}Nb_{0.481}(4^+)$	− 0.00052
	3	7	13/2	$^{92}Nb_{0.481}(4^+)$	0.00639
$^{89}Y_{1.745}(5/2^-)$	4	5	7/2	$^{92}Nb_{0.501}(6^+)$	− 0.00061
	4	5	9/2	$^{92}Nb_{0.501}(6^+)$	0.00133
	4	5	11/2	$^{92}Nb_{0.501}(6^+)$	0.00047
	3	7	13/2	$^{92}Nb_{0.501}(6^+)$	− 0.00313
	3	7	15/2	$^{92}Nb_{0.501}(6^+)$	− 0.00064
	2	9	17/2	$^{92}Nb_{0.501}(6^+)$	− 0.01235
	6	1	1/2	$^{92}Nb_{1.346}(2^+)$	− 0.00010
	6	1	3/2	$^{92}Nb_{1.346}(2^+)$	− 0.00013
	5	3	5/2	$^{92}Nb_{1.346}(2^+)$	0.00004
	5	3	7/2	$^{92}Nb_{1.346}(2^+)$	0.00015
	4	5	9/2	$^{92}Nb_{1.346}(2^+)$	− 0.00064
	4	6	13/2	$^{92}Nb_{2.088}(9^-)$	− 0.00028
	3	8	15/2	$^{92}Nb_{2.088}(9^-)$	0.00067
	3	8	17/2	$^{92}Nb_{2.088}(9^-)$	0.00045
	2	10		$^{92}Nb_{2.088}(9^-)$	− 0.00167

Table 5 continued

Initial state	N	L	J	Final state	S.A.
			19/2		
	2	10	21/2	^{92}Nb$_{2.088}(9^{-})$	− 0.00085
	1	12	23/2	^{92}Nb$_{2.088}(9^{-})$	0.00999
	3	7	13/2	^{92}Nb$_{2.287}(9^{+})$	0.00004
	4	7	13/2	^{92}Nb$_{2.287}(9^{+})$	− 0.00004
	3	7	15/2	^{92}Nb$_{2.287}(9^{+})$	− 0.00014
	2	9	17/2	^{92}Nb$_{2.287}(9^{+})$	0.00010
	3	9	17/2	^{92}Nb$_{2.287}(9^{+})$	0.00012
	3	9	19/2	^{92}Nb$_{2.287}(9^{+})$	0.00021
	2	11	21/2	^{92}Nb$_{2.287}(9^{+})$	0.00008
	2	11	21/2	^{92}Nb$_{2.287}(9^{+})$	0.00003

Appendix B: Spectroscopic amplitudes for $<^{89}\mathrm{Y}|^{92}\mathrm{Zr}>$ overlaps, in the ^{3}H cluster transfer

See Table 6.

Table 6 ^{3}H-spectroscopic amplitudes for the target overlaps used in CRC calculation, where $\overline{N}$, N, L, and J are the number of nodes, principal quantum number, orbital angular momentum, and total angular momentum of the ^{3}H cluster, respectively

Initial state	$\overline{N} = (N+1)$	L	J	Final state	S.A.
^{89}Y$_{g.s.}(1/2^{-})$	6	1	1/2	^{92}Zr$_{g.s.}(0^{+})$	− 0.00758
	7	1	1/2	^{92}Zr$_{g.s.}(0^{+})$	− 0.00029
	6	1	3/2	^{92}Zr$_{0.934}(2^{+})$	0.00812
	7	1	3/2	^{92}Zr$_{0.934}(2^{+})$	0.00026
	5	3	5/2	^{92}Zr$_{0.934}(2^{+})$	− 0.00644
	6	3	5/2	^{92}Zr$_{0.934}(2^{+})$	− 0.00013
	4	5	11/2	^{92}Zr$_{2.937}(6^{+})$	− 0.00223
	5	5	11/2	^{92}Zr$_{2.937}(6^{+})$	− 0.00000333
	3	7	13/2	^{92}Zr$_{2.937}(6^{+})$	0.00210
	4	7	13/2	^{92}Zr$_{2.937}(6^{+})$	0.00018
	4	6	13/2	^{92}Zr$_{3.379}(7^{-})$	− 0.002654
	5	6	13/2	^{92}Zr$_{3.379}(7^{-})$	− 0.000009
	3	8	15/2	^{92}Zr$_{3.379}(7^{-})$	0.004635
	4	8	15/2	^{92}Zr$_{3.379}(7^{-})$	− 0.000013
	5	3	7/2	^{92}Zr$_{1.495}(4^{+})$	0.00674
	6	3	7/2	^{92}Zr$_{1.495}(4^{+})$	0.00015
	4	5	9/2	^{92}Zr$_{1.495}(4^{+})$	− 0.00706
	5	5	9/2	^{92}Zr$_{1.495}(4^{+})$	− 0.00010
	5	4	9/2	^{92}Zr$_{2.486}(5^{-})$	0.006130
	6	4	9/2	^{92}Zr$_{2.486}(5^{-})$	0.000263
	4	6	11/2	^{92}Zr$_{2.486}(5^{-})$	0.000157

Table 6 continued

Initial state	$\overline{N} = (N+1)$	L	J	Final state	S.A.
	5	6	11/2	$^{92}Zr_{2.486}(5^-)$	0.000003
$^{89}Y_{0.909}(9/2^+)$	5	4	9/2	$^{92}Zr_{g.s.}(0^+)$	0.002779
	6	4	9/2	$^{92}Zr_{g.s.}(0^+)$	0.000110
	6	2	5/2	$^{92}Zr_{0.934}(2^+)$	0.002429
	7	2	5/2	$^{92}Zr_{0.934}(2^+)$	0.000032
	5	4	7/2	$^{92}Zr_{0.934}(2^+)$	− 0.001021
	6	4	7/2	$^{92}Zr_{0.934}(2^+)$	− 0.000025
	5	4	9/2	$^{92}Zr_{0.934}(2^+)$	− 0.004250
	6	4	9/2	$^{92}Zr_{0.9346}(2^+)$	− 0.000177
	4	6	11/2	$^{92}Zr_{0.934}(2^+)$	0.002043
	5	6	11/2	$^{92}Zr_{0.934}(2^+)$	0.000090
	4	6	13/2	$^{92}Zr_{0.934}(2^+)$	0.003291
	5	6	11/2	$^{92}Zr_{0.934}(2^+)$	0.000058
	6	2	3/2	$^{92}Zr_{2.937}(6^+)$	− 0.002665
	7	2	3/2	$^{92}Zr_{2.937}(6^+)$	− 0.000024
	6	2	5/2	$^{92}Zr_{2.937}(6^+)$	− 0.003829
	7	2	5/2	$^{92}Zr_{2.937}(6^+)$	− 0.000046
	5	4	7/2	$^{92}Zr_{2.937}(6^+)$	0.001515
	6	4	7/2	$^{92}Zr_{2.937}(6^+)$	0.000020
	5	4	9/2	$^{92}Zr_{2.937}(6^+)$	0.006338
	6	4	9/2	$^{92}Zr_{2.937}(6^+)$	0.000221
	4	6	11/2	$^{92}Zr_{2.937}(6^+)$	− 0.001443
	5	6	11/2	$^{92}Zr_{2.937}(6^+)$	− 0.000052
	4	6	13/2	$^{92}Zr_{2.937}(6^+)$	− 0.004104
$^{89}Y_{0.909}(9/2^+)$	5	6	13/2	$^{92}Zr_{2.937}(6^+)$	− 0.000079
	3	8	15/2	$^{92}Zr_{2.937}(6^+)$	0.001152
	4	8	15/2	$^{92}Zr_{2.937}(6^+)$	0.000044
	3	8	17/2	$^{92}Zr_{2.937}(6^+)$	0.003566
	4	8	17/2	$^{92}Zr_{2.937}(6^+)$	0.000047
	2	10	19/2	$^{92}Zr_{2.937}(6^+)$	− 0.001263
	3	10	19/2	$^{92}Zr_{2.937}(6^+)$	− 0.000043
	2	10	21/2	$^{92}Zr_{2.937}(6^+)$	− 0.006376
	3	10	21/2	$^{92}Zr_{2.937}(6^+)$	− 0.000057
	5	3	5/2	$^{92}Zr_{3.379}(7^-)$	− 0.001818
	6	3	5/2	$^{92}Zr_{3.379}(7^-)$	− 0.000869
	5	3	7/2	$^{92}Zr_{3.379}(7^-)$	− 0.000569
	6	3	7/2	$^{92}Zr_{3.379}(7^-)$	− 0.000673
	4	5	9/2	$^{92}Zr_{3.379}(7^-)$	0.000763
	5	5	9/2	$^{92}Zr_{3.379}(7^-)$	0.000552
	4	5	11/2	$^{92}Zr_{3.379}(7^-)$	0.000564
	5	5	11/2	$^{92}Zr_{3.379}(7^-)$	0.000469
	3	7	13/2	$^{92}Zr_{3.379}(7^-)$	0.000063
	4	7	13/2	$^{92}Zr_{3.379}(7^-)$	− 0.000571
	3	7	15/2	$^{92}Zr_{3.379}(7^-)$	− 0.000142
	4	7	15/2	$^{92}Zr_{3.379}(7^-)$	− 0.000596
	3	9	17/2	$^{92}Zr_{3.379}(7^-)$	0.000831

Table 6 continued

Initial state	$\overline{N} = (N+1)$	L	J	Final state	S.A.
	3	9	19/2	$^{92}Zr_{3.379}(7^-)$	0.001168
	4	11	21/2	$^{92}Zr_{3.379}(7^-)$	− 0.002091
	2	11	23/2	$^{92}Zr_{3.379}(7^-)$	− 0.004758
	7	0	1/2	$^{92}Zr_{1.495}(4^+)$	0.003359
	8	0	1/2	$^{92}Zr_{1.495}(4^+)$	0.000265
	6	2	3/2	$^{92}Zr_{1.495}(4^+)$	− 0.001337
	7	2	3/2	$^{92}Zr_{1.495}(4^+)$	− 0.000013
	6	2	5/2	$^{92}Zr_{1.495}(4^+)$	− 0.002212
	7	2	5/2	$^{92}Zr_{1.495}(4^+)$	− 0.000023
	5	4	7/2	$^{92}Zr_{1.495}(4^+)$	0.001281
	6	4	7/2	$^{92}Zr_{1.495}(4^+)$	0.000018
	5	4	9/2	$^{92}Zr_{1.495}(4^+)$	0.003014
	6	4	9/2	$^{92}Zr_{1.495}(4^+)$	0.000092
	4	6	11/2	$^{92}Zr_{1.495}(4^+)$	− 0.001660
	5	6	11/2	$^{92}Zr_{1.495}(4^+)$	− 0.000058
	4	6	13/2	$^{92}Zr_{1.495}(4^+)$	− 0.002775
	5	6	13/2	$^{92}Zr_{1.495}(4^+)$	− 0.000051
	3	8	15/2	$^{92}Zr_{1.495}(4^+)$	0.002218
	4	8	15/2	$^{92}Zr_{1.495}(4^+)$	0.000048
	3	8	17/2	$^{92}Zr_{1.495}(4^+)$	0.004669
	4	8	17/2	$^{92}Zr_{1.495}(4^+)$	0.000043
	6	1	1/2	$^{92}Zr_{2.486}(5^-)$	− 0.02179
	7	1	1/2	$^{92}Zr_{2.486}(5^-)$	− 0.00098
	6	1	3/2	$^{92}Zr_{2.486}(5^-)$	0.00113
	7	1	3/2	$^{92}Zr_{2.486}(5^-)$	− 0.00012
	5	3	5/2	$^{92}Zr_{2.486}(5^-)$	0.00357
	6	3	5/2	$^{92}Zr_{2.486}(5^-)$	0.00008
	5	3	7/2	$^{92}Zr_{2.486}(5^-)$	− 0.00014
	6	3	7/2	$^{92}Zr_{2.486}(5^-)$	0.00003
	4	5	9/2	$^{92}Zr_{2.486}(5^-)$	− 0.00119
	5	5	9/2	$^{92}Zr_{2.486}(5^-)$	− 0.00004
	4	5	11/2	$^{92}Zr_{2.486}(5^-)$	− 0.000042
	5	5	11/2	$^{92}Zr_{2.486}(5^-)$	− 0.00003
	3	7	13/2	$^{92}Zr_{2.486}(5^-)$	0.000197
	4	7	13/2	$^{92}Zr_{2.486}(5^-)$	0.000046
	3	7	15/2	$^{92}Zr_{2.486}(5^-)$	0.000008
	4	7	15/2	$^{92}Zr_{2.486}(5^-)$	0.000058
	2	9	17/2	$^{92}Zr_{2.486}(5^-)$	0.000082
	3	9	17/2	$^{92}Zr_{2.486}(5^-)$	− 0.000043
	3	9	19/2	$^{92}Zr_{2.486}(5^-)$	− 0.000021
$^{89}Y_{1.507}(3/2^-)$	6	1	3/2	$^{92}Zr_{g.s.}(0^+)$	− 0.014033
	7	1	3/2	$^{92}Zr_{g.s.}(0^+)$	− 0.000911
	6	1	1/2	$^{92}Zr_{0.934}(2^+)$	0.009907
	7	1	1/2	$^{92}Zr_{0.934}(2^+)$	0.000425
	6	1	3/2	$^{92}Zr_{0.934}(2^+)$	0.012099
	7	1	3/2	$^{92}Zr_{0.934}(2^+)$	0.000551

Table 6 continued

Initial state	$\overline{N} = (N+1)$	L	J	Final state	S.A.
	5	3	5/2	$^{92}Zr_{0.934}(2^+)$	− 0.012022
	6	3	5/2	$^{92}Zr_{0.934}(2^+)$	− 0.000506
	5	3	7/2	$^{92}Zr_{0.934}(2^+)$	− 0.012295
	6	3	7/2	$^{92}Zr_{0.934}(2^+)$	− 0.000489
	4	5	9/2	$^{92}Zr_{2.937}(6^+)$	− 0.002941
	5	5	9/2	$^{92}Zr_{2.937}(6^+)$	− 0.000117
	4	5	11/2	$^{92}Zr_{2.937}(6^+)$	− 0.004086
	5	5	11/2	$^{92}Zr_{2.937}(6^+)$	− 0.000157
	3	7	13/2	$^{92}Zr_{2.937}(6^+)$	0.005289
	4	7	13/2	$^{92}Zr_{2.937}(6^+)$	0.000223
	3	7	15/2	$^{92}Zr_{2.937}(6^+)$	0.005958
	4	7	15/2	$^{92}Zr_{2.937}(6^+)$	0.000231
	4	6	11/2	$^{92}Zr_{3.379}(7^-)$	− 0.004419
	5	6	11/2	$^{92}Zr_{3.379}(7^-)$	− 0.000018
	4	6	13/2	$^{92}Zr_{3.379}(7^-)$	− 0.005011
	5	6	13/2	$^{92}Zr_{3.379}(7^-)$	− 0.000023
	3	8	15/2	$^{92}Zr_{3.379}(7^-)$	0.008506
	4	8	15/2	$^{92}Zr_{3.379}(7^-)$	0.000031
	2	8	17/2	$^{92}Zr_{3.379}(7^-)$	0.010021
	4	8	17/2	$^{92}Zr_{3.379}(7^-)$	0.000047
	5	3	5/2	$^{92}Zr_{1.495}(4^+)$	0.008443
	6	3	5/2	$^{92}Zr_{1.495}(4^+)$	0.000405
	5	3	7/2	$^{92}Zr_{1.495}(4^+)$	0.009877
	6	3	7/2	$^{92}Zr_{1.495}(4^+)$	0.000398
	4	5	9/2	$^{92}Zr_{1.495}(4^+)$	− 0.011693
	5	5	9/2	$^{92}Zr_{1.495}(4^+)$	− 0.000383
	4	5	11/2	$^{92}Zr_{1.495}(4^+)$	− 0.01231
	5	5	11/2	$^{92}Zr_{1.495}(4^+)$	− 0.000360
	5	4	7/2	$^{92}Zr_{2.486}(5^-)$	0.000446
	6	4	7/2	$^{92}Zr_{2.486}(5^-)$	0.000006
	5	4	9/2	$^{92}Zr_{2.486}(5^-)$	− 0.000268
	6	4	9/2	$^{92}Zr_{2.486}(5^-)$	− 0.000012
	4	6	11/2	$^{92}Zr_{2.486}(5^-)$	− 0.000148
	5	6	11/2	$^{92}Zr_{2.486}(5^-)$	− 0.000015
	4	6	13/2	$^{92}Zr_{2.486}(5^-)$	0.001335
	5	6	13/2	$^{92}Zr_{2.486}(5^-)$	0.000027
$^{89}Y_{1.745}(5/2^-)$	5	3	5/2	$^{92}Zr_{g.s.}(0^+)$	0.007518
	6	3	5/2	$^{92}Zr_{g.s.}(0^+)$	0.000244
	6	1	1/2	$^{92}Zr_{2.486}(2^+)$	0.008055
	7	1	1/2	$^{92}Zr_{2.486}(2^+)$	0.000208
	6	1	3/2	$^{92}Zr_{2.486}(2^+)$	0.006533
	7	1	3/2	$^{92}Zr_{2.486}(2^+)$	0.000201
	5	3	5/2	$^{92}Zr_{2.486}(2^+)$	− 0.005059
	6	3	5/2	$^{92}Zr_{2.486}(2^+)$	− 0.000070
	5	3	7/2	$^{92}Zr_{2.486}(2^+)$	− 0.005351
	6	3	7/2	$^{92}Zr_{2.486}(2^+)$	− 0.000113

Table 6 continued

Initial state	$\overline{N} = (N+1)$	L	J	Final state	S.A.
	4	5	9/2	$^{92}Zr_{2.486}(2^+)$	0.008511
	5	5	9/2	$^{92}Zr_{2.486}(2^+)$	0.000116
	5	3	7/2	$^{92}Zr_{2.937}(6^+)$	0.001309
	6	3	7/2	$^{92}Zr_{2.937}(6^+)$	0.000047
	4	5	9/2	$^{92}Zr_{2.937}(6^+)$	− 0.001624
	5	5	9/2	$^{92}Zr_{2.937}(6^+)$	− 0.000020
	4	5	11/2	$^{92}Zr_{2.937}(6^+)$	− 0.001613
	5	5	11/2	$^{92}Zr_{2.937}(6^+)$	− 0.000037
	3	7	13/2	$^{92}Zr_{2.937}(6^+)$	0.002893
	4	7	13/2	$^{92}Zr_{2.937}(6^+)$	0.000040
	3	7	15/2	$^{92}Zr_{2.937}(6^+)$	0.002545
	4	7	15/2	$^{92}Zr_{2.937}(6^+)$	0.000059
	2	9	17/2	$^{92}Zr_{2.937}(6^+)$	− 0.006404
	3	9	17/2	$^{92}Zr_{2.937}(6^+)$	− 0.000077
	5	4	9/2	$^{92}Zr_{3.379}(7^-)$	0.002049
	6	4	9/2	$^{92}Zr_{3.379}(7^-)$	0.000021
	4	6	11/2	$^{92}Zr_{3.379}(7^-)$	− 0.001944
	5	6	11/2	$^{92}Zr_{3.379}(7^-)$	− 0.000006
	4	6	13/2	$^{92}Zr_{3.379}(7^-)$	− 0.002306
	5	6	13/2	$^{92}Zr_{3.379}(7^-)$	− 0.000003
	3	8	15/2	$^{92}Zr_{3.379}(7^-)$	0.004232
	4	8	15/2	$^{92}Zr_{3.379}(7^-)$	− 0.000002
	3	8	17/2	$^{92}Zr_{3.379}(7^-)$	0.004307
	4	8	17/2	$^{92}Zr_{3.379}(7^-)$	0.000004
	2	10	19/2	$^{92}Zr_{3.379}(7^-)$	− 0.009513
	3	10	19/2	$^{92}Zr_{3.379}(7^-)$	0.000029
$^{89}Y_{1.745}(5/2^-)$	6	1	3/2	$^{92}Zr_{1.495}(4^+)$	− 0.005354
	7	1	3/2	$^{92}Zr_{1.495}(4^+)$	− 0.000174
	5	3	5/2	$^{92}Zr_{1.495}(4^+)$	0.004344
	6	3	5/2	$^{92}Zr_{1.495}(4^+)$	0.000047
	5	3	7/2	$^{92}Zr_{1.495}(4^+)$	0.004091
	6	3	7/2	$^{92}Zr_{1.495}(4^+)$	0.0000358
	4	5	9/2	$^{92}Zr_{1.495}(4^+)$	− 0.005423
	5	5	9/2	$^{92}Zr_{1.495}(4^+)$	− 0.000017
	4	5	11/2	$^{92}Zr_{1.495}(4^+)$	− 0.005241
	5	5	11/2	$^{92}Zr_{1.495}(4^+)$	− 0.000048
	3	7	13/2	$^{92}Zr_{1.495}(4^+)$	0.010810
	4	7	13/2	$^{92}Zr_{1.495}(4^+)$	0.000039
	6	2	5/2	$^{92}Zr_{2.486}(5^-)$	0.000454
	7	2	5/2	$^{92}Zr_{2.486}(5^-)$	0.000010
	5	4	7/2	$^{92}Zr_{2.486}(5^-)$	0.000218
	6	4	7/2	$^{92}Zr_{2.486}(5^-)$	0.000011
	5	4	9/2	$^{92}Zr_{2.486}(5^-)$	− 0.000450
	6	4	9/2	$^{92}Zr_{2.486}(5^-)$	− 0.000027
	4	6	11/2	$^{92}Zr_{2.486}(5^-)$	− 0.000100
	5	6	11/2	$^{92}Zr_{2.486}(5^-)$	− 0.000018

Table 6 continued

Initial state	$\overline{N} = (N+1)$	L	J	Final state	S.A.
	4	6	13/2	$^{92}Zr_{2.486}(5^-)$	0.000469
	5	6	13/2	$^{92}Zr_{2.486}(5^-)$	0.000012
	3	8	15/2	$^{92}Zr_{2.486}(5^-)$	− 0.000082
	4	8	15/2	$^{92}Zr_{2.486}(5^-)$	0.000001

Appendix C: Spectroscopic amplitudes for $<^{89}Y|^{91}Zr>$, $<^{91}Zr|^{92}Nb>$, and $<^{91}Zr|^{92}Zr>$ overlaps, for the sequential ^{3}He and ^{3}H transfer

See Tables 7, 8, and 9.

Table 7 Spectroscopic amplitudes for deuteron-like transfer reactions

Initial state	$(n_1l_1j_1)$ $(n_2l_2j_2)$	Final state	J_{12}	S.A.
$^{89}Y_{g.s.}$ $(1/2)^-$	$(1g_{7/2})$ $(1f_{5/2})$	$^{91}Zr_{g.s.}(5/2)^+$	2	− 0.0008
	$(1g_{7/2})$ $(2p_{3/2})$			− 0.0026
	$(2d_{5/2})$ $(1f_{5/2})$			− 0.0010
	$(2d_{5/2})$ $(2p_{3/2})$			− 0.0220
	$(2d_{5/2})$ $(2p_{1/2})$			0.7334
	$(2d_{3/2})$ $(1f_{5/2})$			0.0001
	$(2d_{3/2})$ $(2p_{3/2})$			− 0.0074
	$(2d_{3/2})$ $(2p_{1/2})$			− 0.0002
	$(3s_{1/2})$ $(1f_{5/2})$			− 0.0013
	$(3s_{1/2})$ $(2p_{3/2})$			− 0.0094
	$(1h_{11/2})$ $(1g_{9/2})$			0.0417
	$(1g_{7/2})$ $(1f_{5/2})$		3	0.0015
	$(1g_{7/2})$ $(2p_{3/2})$			0.0023
	$(2d_{5/2})$ $(1f_{5/2})$			− 0.0008
	$(2d_{5/2})$ $(2p_{3/2})$			0.0117
	$(2d_{5/2})$ $(2p_{1/2})$			0.8680
	$(2d_{3/2})$ $(1f_{5/2})$			− 0.0009
	$(2d_{3/2})$ $(2p_{3/2})$			0.0047
	$(1h_{11/2})$ $(1g_{9/2})$			− 0.0385
$^{89}Y_{g.s.}(1/2)^-$	$(1g_{7/2})(1f_{5/2})$	$^{91}Zr_{1.2048}(1/2)^+$	0	− 0.0010
	$(2d_{3/2})$ $(2p_{3/2})$			0.0185
	$(3s_{1/2})$ $(2p_{1/2})$			− 0.5377
	$(1g_{7/2})$ $(1f_{5/2})$		1	0.0025
	$(2d_{5/2})$ $(1f_{5/2})$			0.0039
	$(2d_{5/2})$ $(2p_{3/2})$			− 0.0301
	$(2d_{3/2})$ $(1f_{5/2})$			0.0008

Table 7 continued

Initial state	$(n_1l_1j_1)$ $(n_2l_2j_2)$	Final state	J_{12}	S.A.
	$(2d_{3/2})$ $(2p_{3/2})$			− 0.0048
	$(2d_{3/2})$ $(2p_{1/2})$			0.0006
	$(3s_{1/2})$ $(2p_{3/2})$			− 0.0008
	$(3s_{1/2})$ $(2p_{1/2})$			− 0.9315
	$(1h_{11/2})$ $(1g_{9/2})$			0.1404
$^{89}Y_{g.s.}(1/2)^-$	$(1g_{7/2})$ $(1g_{9/2})$	$^{91}Zr_{1.2048}(1/2)^+$	4	0.0545
	$(2d_{5/2})$ $(1g_{9/2})$			− 0.1830
	$(2d_{3/2})$ $(1g_{9/2})$			0.1476
	$(3s_{1/2})$ $(1g_{9/2})$			− 0.6452
	$(1h_{11/2})$ $(1f_{5/2})$			0.0003
	$(1h_{11/2})$ $(2p_{3/2})$			− 0.0005
	$(1g_{7/2})$ $(1g_{9/2})$		5	− 0.0359
	$(2d_{5/2})$ $(1g_{9/2})$			− 0.2497
	$(2d_{3/2})$ $(1g_{9/2})$			− 0.1194
	$(3s_{1/2})$ $(1g_{9/2})$			− 0.7139
	$(1h_{11/2})$ $(1f_{5/2})$			− 0.0076
	$(1h_{11/2})$ $(2p_{3/2})$			− 0.0153
	$(1h_{11/2})$ $(2p_{1/2})$			0.1288
$^{89}Y_{g.s.}(1/2)^-$	$(1g_{7/2})(1f_{5/2})$	$^{91}Zr_{1.8822}(7/2)^+$	3	0.0034
	$(1g_{7/2})(2p_{3/2})$			0.0225
	$(1g_{7/2})(2p_{1/2})$			− 0.3124
	$(2d_{5/2})(1f_{5/2})$			− 0.0005
	$(2d_{5/2})(2p_{3/2})$			− 0.0165
	$(2d_{5/2})(2p_{1/2})$			0.0010
	$(2d_{3/2})(1f_{5/2})$			− 0.0022
	$(2d_{3/2})(2p_{3/2})$			0.0162
	$(3s_{1/2})(1f_{5/2})$			0.0007
	$(1h_{11/2})(1g_{9/2})$			0.0263
	$(1g_{7/2})(1f_{5/2})$		4	0.0041
	$(1g_{7/2})(2p_{3/2})$			− 0.0176
	$(1g_{7/2})(2p_{1/2})$			− 0.3547
	$(2d_{5/2})(1f_{5/2})$			− 0.0063
	$(2d_{5/2})(2p_{3/2})$			0.0094
	$(2d_{3/2})(1f_{5/2})$			− 0.0027
	$(1h_{11/2})(1g_{9/2})$			− 0.0105

Table 7 continued

Initial state	$(n_1l_1j_1)$ $(n_2l_2j_2)$	Final state	J_{12}	S.A.
$^{89}Y_{0.909}(9/2)^+$	$(1g_{7/2})(1g_{9/2})$	$^{91}Zr_{g.s.}(5/2)^+$	2	− 0.0463
	$(2d_{5/2})(1g_{9/2})$			0.3675
	$(2d_{5/2})(1g_{9/2})$		3	0.3010
	$(2d_{3/2})(1g_{9/2})$			0.0577
	$(1h_{11/2})(1f_{5/2})$			− 0.0025
	$(1g_{7/2})(1g_{9/2})$		4	− 0.0174
	$(2d_{5/2})(1g_{9/2})$			0.2913
	$(2d_{3/2})(1g_{9/2})$			− 0.0192
	$(3s_{1/2})(1g_{9/2})$			0.0471
	$(1h_{11/2})(1f_{5/2})$			0.0004
	$(1h_{11/2})(2p_{3/2})$			0.0038
	$(1g_{7/2})(1g_{9/2})$		5	0.0129
	$(2d_{5/2})(1g_{9/2})$			0.3191
	$(2d_{3/2})(1g_{9/2})$			0.0291
	$(3s_{1/2})(1g_{9/2})$			0.0642
	$(1h_{11/2})(1f_{5/2})$			− 0.0015
	$(1h_{11/2})(2p_{3/2})$			0.0100
	$(1h_{11/2})(2p_{1/2})$			− 0.0478
$^{89}Y_{0.909}(9/2)^+$	$(1g_{7/2})(1f_{5/2})$	$^{91}Zr_{1.2048}(1/2)^+$	4	0.0545
	$(1g_{7/2})(2p_{3/2})$			0.0225
	$(1g_{7/2})(2p_{1/2})$			− 0.3124
	$(2d_{5/2})(1f_{5/2})$			− 0.0005
	$(2d_{5/2})(2p_{3/2})$			− 0.0165
	$(2d_{5/2})(2p_{1/2})$			0.0010
	$(2d_{3/2})(1f_{5/2})$			− 0.0022
	$(2d_{3/2})(2p_{3/2})$			0.0162
	$(3s_{1/2})(1f_{5/2})$			0.0007
	$(1h_{11/2})(1g_{9/2})$			0.0263
$^{89}Y_{1.507}(3/2)^-$	$(1g_{7/2})(1g_{9/2})$	$^{91}Zr_{g.s.}(5/2)^+$	2	− 0.0463
	$(2d_{5/2})(1g_{9/2})$			0.3675
	$(2d_{5/2})(1g_{9/2})$		3	0.3010
	$(2d_{3/2})(1g_{9/2})$			0.0577
	$(1h_{11/2})(1f_{5/2})$			− 0.0025
	$(1g_{7/2})(1g_{9/2})$		4	− 0.0174
	$(2d_{5/2})(1g_{9/2})$			0.2913
	$(2d_{3/2})(1g_{9/2})$			− 0.0192
	$(3s_{1/2})(1g_{9/2})$			0.0471
	$(1h_{11/2})(1f_{5/2})$			− 0.0015
	$(1h_{11/2})(2p_{3/2})$			0.0038
	$(1g_{7/2})(1g_{9/2})$		5	0.0129
	$(2d_{5/2})(1g_{9/2})$			0.3191
	$(2d_{3/2})(1g_{9/2})$			0.0291
	$(3s_{1/2})(1g_{9/2})$			0.0642
	$(1h_{11/2})(1f_{5/2})$			− 0.0015
	$(1h_{11/2})(2p_{3/2})$			0.0100
	$(1h_{11/2})(2p_{1/2})$			− 0.0478
$^{89}Y_{0.909}(9/2)^+$	$(1g_{7/2})(1f_{5/2})$	$^{91}Zr_{1.2048}(1/2)^+$	4	0.0545
	$(1g_{7/2})(2p_{3/2})$			0.0225
	$(1g_{7/2})(2p_{1/2})$			− 0.3124
	$(2d_{5/2})(1f_{5/2})$			− 0.0005
	$(2d_{5/2})(2p_{3/2})$			− 0.0165
	$(2d_{5/2})(2p_{1/2})$			0.0010
	$(2d_{3/2})(1f_{5/2})$			− 0.0022
	$(2d_{3/2})(2p_{3/2})$			0.0162
	$(3s_{1/2})(1f_{5/2})$			0.0007
	$(1h_{11/2})(1g_{9/2})$			0.0263
$^{89}Y_{1.507}(3/2)^-$	$(1g_{7/2})(1g_{9/2})$	$^{91}Zr_{g.s.}(5/2)^+$	2	− 0.0463
	$(2d_{5/2})(1g_{9/2})$			0.3675
	$(2d_{5/2})(1g_{9/2})$		3	0.3010
	$(2d_{3/2})(1g_{9/2})$			0.0577
	$(1h_{11/2})(1f_{5/2})$			− 0.0025
	$(1g_{7/2})(1g_{9/2})$		4	− 0.0174
	$(2d_{5/2})(1g_{9/2})$			0.2913
	$(2d_{3/2})(1g_{9/2})$			− 0.0192
	$(3s_{1/2})(1g_{9/2})$			0.0471
	$(1h_{11/2})(1f_{5/2})$			− 0.0015
	$(1h_{11/2})(2p_{3/2})$			0.0038
	$(1g_{7/2})(1g_{9/2})$		5	0.0129
	$(2d_{5/2})(1g_{9/2})$			0.3191
	$(2d_{3/2})(1g_{9/2})$			0.0291
	$(3s_{1/2})(1g_{9/2})$			0.0642
	$(1h_{11/2})(1f_{5/2})$			− 0.0015
	$(1h_{11/2})(2p_{3/2})$			0.0100
	$(1h_{11/2})(2p_{1/2})$			− 0.0478
$^{89}Y_{0.909}(9/2)^+$	$(1g_{7/2})(1f_{5/2})$	$^{91}Zr_{1.2048}(1/2)^+$	4	0.0545
	$(1g_{7/2})(2p_{3/2})$			0.0225
	$(1g_{7/2})(2p_{1/2})$			− 0.3124
	$(2d_{5/2})(1f_{5/2})$			− 0.0005
	$(2d_{5/2})(2p_{3/2})$			− 0.0165
	$(2d_{5/2})(2p_{1/2})$			0.0010
	$(2d_{3/2})(1f_{5/2})$			− 0.0022
	$(2d_{3/2})(2p_{3/2})$			0.0162
	$(3s_{1/2})(1f_{5/2})$			0.0007
	$(1h_{11/2})(1g_{9/2})$			0.0263

In the second column, the first orbital, which corresponds to $n_1l_1j_1$, is related to neutrons, and the second orbital, $n_2l_2j_2$, to protons

Table 8 Spectroscopic amplitudes for a single proton transfer in ^{91}Zr (^{4}He, ^{3}H) ^{92}Nb reaction

Initial state	N	L	J	Final state	S.A.
$^{91}Zr_{g.s.}(5/2)^+$	1	4	9/2	$^{92}Nb_{g.s.}(7)^+$	0.8555
	2	4	9/2	$^{92}Nb_{0.1360}(2)^+$	0.81393
	1	4	9/2	$^{92}Nb_{0.2857}(3)^+$	0.8228
	1	4	9/2	$^{92}Nb_{0.3574}(5)^+$	− 0.8034
	1	4	9/2	$^{92}Nb_{0.4805}(4)^+$	− 0.8462
	1	4	9/2	$^{92}Nb_{0.5010}(6)^+$	− 0.8769
	1	4	9/2	$^{92}Nb_{1.3455}(2)^+$	0.0375
$^{91}Zr_{1.2048}(1/2)^+$	1	4	9/2	$^{92}Nb_{0.3574}(5)^+$	0.2623
	1	4	9/2	$^{92}Nb_{0.4805}(4)^+$	0.1639
$^{91}Zr_{1.4664}(5/2)^+$	1	4	9/2	$^{92}Nb_{g.s.}(7)^+$	− 0.3539
	2	4	9/2	$^{92}Nb_{0.1360}(2)^+$	− 0.3545
	1	4	9/2	$^{92}Nb_{0.2857}(3)^+$	− 0.3004
	1	4	9/2	$^{92}Nb_{0.3574}(5)^+$	0.2897
	1	4	9/2	$^{92}Nb_{0.4805}(4)^+$	0.2902
	1	4	9/2	$^{92}Nb_{0.5010}(6)^+$	0.2692
	1	4	9/2	$^{92}Nb_{1.3455}(2)^+$	0.3946
$^{91}Zr_{1.8822}(7/2)^+$	1	4	9/2	$^{92}Nb_{g.s.}(7)^+$	0.0260
	2	4	9/2	$^{92}Nb_{0.1360}(2)^+$	− 0.0299
	1	4	9/2	$^{92}Nb_{0.2857}(3)^+$	− 0.0371
	1	4	9/2	$^{92}Nb_{0.3574}(5)^+$	0.0013
	1	4	9/2	$^{92}Nb_{0.4805}(4)^+$	0.0299
	1	4	9/2	$^{92}Nb_{0.5010}(6)^+$	0.0348
	1	4	9/2	$^{92}Nb_{1.3455}(2)^+$	0.1861

Table 9 Spectroscopic amplitudes for a single neutron transfer in ^{91}Zr (^{4}He, ^{3}He) ^{92}Zr reaction

Initial state	N	L	J	Final state	S.A.
$^{91}Zr_{g.s.}(5/2)^+$	2	2	5/2	$^{92}Zr_{g.s.}(0)^+$	1.0657
	3	0	1/2	$^{92}Zr_{0.9345}(2)^+$	0.2650
	2	2	3/2	$^{92}Zr_{1.4955}(4)^+$	0.3277
	1	5	11/2	$^{92}Zr_{2.4860}(5)^-$	0.0195
	1	4	7/2	$^{92}Zr_{2.9574}(6)^+$	0.4445
	1	5	11/2	$^{92}Zr_{3.3790}(7)^-$	0.8229
$^{91}Zr_{1.2048}(1/2)^+$	3	0	1/2	$^{92}Zr_{g.s.}(0)^+$	0.2746
	2	2	3/2	$^{92}Zr_{0.9345}(2)^+$	0.1531
	1	4	7/2	$^{92}Zr_{1.4955}(4)^+$	0.0959
	1	5	11/2	$^{92}Zr_{2.4860}(5)^-$	− 0.0068
$^{91}Zr_{1.4664}(5/2)^+$	2	2	5/2	$^{91}Zr_{g.s.}(5/2)^+$	0.1758
	3	0	1/2	$^{92}Zr_{0.9345}(2)^+$	0.0673
	2	2	3/2	$^{92}Zr_{1.4955}(4)^+$	0.1131
	1	5	11/2	$^{92}Zr_{2.4860}(5)^-$	0.0210
	1	4	7/2	$^{92}Zr_{2.9574}(6)^+$	0.3876
	1	5	11/2	$^{92}Zr_{3.3790}(7)^-$	− 0.0471
$^{91}Zr_{1.8822}(7/2)^+$	1	4	7/2	$^{92}Zr_{g.s.}(0)^+$	− 0.3195
	2	2	3/2	$^{92}Zr_{0.9345}(2)^+$	− 0.1291
	3	0	1/2	$^{92}Zr_{1.4955}(4)^+$	0.1328
	1	5	11/2	$^{92}Zr_{2.4860}(5)^-$	0.0079
	2	2	5/2	$^{92}Zr_{2.9574}(6)^+$	0.6454
	1	5	11/2	$^{92}Zr_{3.3790}(7)^-$	− 0.0024

Acknowledgements We thank the INFN-LNL staff for providing a stable ^{6}Li beam throughout the experiment.

References

1. H. Kumawat, V.V. Parkar, T.N. Nag et al., Experimental evidence for α production following neutron transfer in the ^{13}C+^{93}Nb system. Phys. Rev. C **105**, 024611 (2022). https://doi.org/10.1103/PhysRevC.105.024611
2. T. Otsuka, T. Abe, T. Yoshida et al., α-Clustering in atomic nuclei from first principles with statistical learning and the Hoyle state character. Nat. Commun. **13**, 2234 (2022). https://doi.org/10.1038/s41467-022-29582-0
3. N. Itagaki, S. Aoyama, S. Okabe et al., Cluster-shell competition in light nuclei. Phys. Rev. C **70**, 054307 (2004). https://doi.org/10.1103/PhysRevC.70.054307

4. A. Tohsaki, H. Horiuchi, P. Schuck et al., Alpha cluster Condensation in ^{12}C and ^{16}O. Phys. Rev. Lett. **87**, 192501 (2001). https://doi.org/10.1103/PhysRevLett.87.192501
5. P.E. Hodgson, Alpha-clustering in nuclei. Nature **257**, 446–447 (1975). https://doi.org/10.1038/257446a0
6. D. Kahl, H. Yamaguchi, S. Hayakawa, α Clustering in nuclear astrophysics and topology. AIP Conf. Proc. **11**, 1189040 (2023). https://doi.org/10.3389/fphy.2023.1189040
7. Y.T. Oganessian, V.I. Zagrebaev, J.S. Vaagen, "Di-Neutron'' configuration of ^{6}He. Phys. Rev. Lett. **82**, 4996–4999 (1999). https://doi.org/10.1103/physrevlett.82.4996
8. Y. Kanada-En'yo, The structure of ground and excited states of ^{12}C. Prog. Theor. Phys. **117**, 655–680 (2007). https://doi.org/10.1143/ptp.117.655
9. T. Neff, H. Feldmeier, R. Roth, Nuclear structure of light nuclei in an extended FMD approach. https://www.osti.gov/etdeweb/biblio/20479778 (2004)
10. M. Chernykh, H. Feldmeier, T. Neff et al., Structure of the Hoyle state in ^{12}C. Phys. Rev. Lett. **98**, 032501 (2007). https://doi.org/10.1103/physrevlett.98.032501
11. W. von Oertzen, M. Freer, Y. Kanada-En'yo, Nuclear clusters and nuclear molecules. Phys. Rep. **432**, 43–113 (2006). https://doi.org/10.1016/j.physrep.2006.07.001
12. Y. Liu, Y.L. Ye, J.L. Lou et al., Positive-parity linear-chain molecular band in ^{16}C. Phys. Rev. Lett. **124**, 192501 (2020). https://doi.org/10.1103/PhysRevLett.124.192501
13. J. Chen, Y. Ye, K. Ma et al., New evidence of the Hoyle-like structure in ^{16}O. Sci. Bull. **68**, 1119–1126 (2023). https://doi.org/10.1016/j.scib.2023.04.031
14. E.M. Burbidge, G.R. Burbidge, W.A. Fowler et al., Synthesis of the elements in stars. Rev. Mod. Phys. **29**, 547–650 (1957). https://doi.org/10.1103/RevModPhys.29.547
15. K.J. Cook, E.C. Simpson, L.T. Bezzina et al., Origins of incomplete fusion products and the suppression of complete fusion in reactions of ^{7}Li. Phys. Rev. Lett. **122**, 102501 (2019). https://doi.org/10.1103/PhysRevLett.122.102501
16. J. Lei, A.M. Moro, Puzzle of complete fusion suppression in weakly bound nuclei: A trojan horse effect? Phys. Rev. Lett. **122**, 042503 (2019). https://doi.org/10.1103/PhysRevLett.122.042503
17. G.L. Zhang, G.X. Zhang, S.P. Hu et al., One-neutron stripping processes to excited states of ^{90}Y* in the ^{89}Y(^{6}Li,^{5}Li)^{90}Y* reaction. Phys. Rev. C **223**, 01068 (2019). https://doi.org/10.1051/epjconf/201922301068
18. S.K. Pandit, A. Shrivastava, K. Mahata et al., Investigation of large α production in reactions involving weakly bound ^{7}Li. Phys. Rev. C **96**, 044616 (2017). https://doi.org/10.1103/PhysRevC.96.044616
19. C.S. Palshetkar, S. Santra, A. Shrivastava et al., Elastic scattering and α production in the ^{9}Be +^{89} Y system. Phys. Rev. C **89**, 064610 (2014). https://doi.org/10.1103/PhysRevC.89.064610
20. D. Tilley, C. Cheves, J. Godwin et al., Energy levels of light nuclei $A = 5, 6, 7$. Nucl. Phys. A **708**, 3–163 (2002). https://doi.org/10.1016/S0375-9474(02)00597-3
21. D. Tilley, J. Kelley, J. Godwin et al., Energy levels of light nuclei $A = 8, 9, 10$. Nucl. Phys. A **745**, 155–362 (2004). https://doi.org/10.1016/j.nuclphysa.2004.09.059
22. D. Luong, M. Dasgupta, D. Hinde et al., Insights into the mechanisms and time-scales of breakup of ^{6,7}Li. Phys. Lett. B **695**, 105–109 (2011). https://doi.org/10.1016/j.physletb.2010.11.007
23. Y.J. Yao, C.J. Lin, L. Yang et al., Relative probabilities of breakup channels in reactions of ^{6,7}Li with ^{209}Bi at energies around and above the coulomb barrier*. Chin. Phys. C. **45**, 054104 (2021). https://doi.org/10.1088/1674-1137/abe3ee
24. M. Dasgupta, P.R.S. Gomes, D.J. Hinde et al., Effect of breakup on the fusion of ^{6}Li, ^{7}Li, and ^{9}Be with heavy nuclei. Phys. Rev. C **70**, 024606 (2004). https://doi.org/10.1103/PhysRevC.70.024606
25. S. Bottoni, S. Leoni, B. Fornal et al., Cluster-transfer reactions with radioactive beams: a spectroscopic tool for neutron-rich nuclei. Phys. Rev. C **92**, 024322 (2015). https://doi.org/10.1103/PhysRevC.92.024322
26. V.V. Parkar, V. Jha, S. Kailas, Systematics and mechanisms of α production with weakly and strongly bound projectiles. The Eur. Phys. J. A. **59**, 88 (2023). https://doi.org/10.1140/epja/s10050-023-01011-w
27. J.D. Garrett, H.G. Bingham, H.T. Fortune et al., Study of the reactions ^{16}O (^{6}Li, ^{3}He) ^{19}F and ^{16}O(^{6}Li, t)^{19}Ne at $E(^{6}\mathrm{Li}) = 24$ MeV. Phys. Rev. C **5**, 682–690 (1972). https://doi.org/10.1103/PhysRevC.5.682
28. D. Testov, D. Mengoni, A.E.A. Goasduff, The 4π highly-efficient light-charged-particle detector Euclides, installed at the Galileo array for in-beam γ-ray spectroscopy. Eur. Phys. J. A **55**, 12714 (2019). https://doi.org/10.1140/epja/i2019-12714-6
29. A. Goasduff, D. Mengoni, F. Recchia et al., The Galileo γ-ray array at the Legnaro national laboratories. Nucl. Instrum. Methods A. **1015**, 165753 (2021). https://doi.org/10.1016/j.nima.2021.165753
30. A. Gavron, Statistical model calculations in heavy ion reactions. Phys. Rev. C **21**, 230–236 (1980). https://doi.org/10.1103/PhysRevC.21.230
31. J. Acharya, S. Mukherjee, A. Chatterjee et al., Neutron emission in ^{19}F-induced reactions. Phys. Rev. C **97**, 034607 (2018). https://doi.org/10.1103/PhysRevC.97.034607
32. M. Kildir, G. La Rana, R. Moro et al., Ingoing-wave boundary condition versus optical model transmission coefficients: a systematic comparison with particle emission data. Phys. Rev. C **51**, 1873–1881 (1995). https://doi.org/10.1103/PhysRevC.51.1873
33. J.I. Thompson, http://www.fresco.org.uk/
34. L.C. Chamon, B.V. Carlson, L.R. Gasques et al., Toward a global description of the nucleus-nucleus interaction. Phys. Rev. C **66**, 014610 (2002). https://doi.org/10.1103/PhysRevC.66.014610
35. D. Pereira, J. Lubian, J. Oliveira et al., An imaginary potential with universal normalization for dissipative processes in heavy-ion reactions. Phys. Lett. B **670**, 330–335 (2009). https://doi.org/10.1016/j.physletb.2008.10.066
36. L. Gasques, L. Chamon, P. Gomes et al., Comparison between heavy-ion reaction and fusion processes for hundreds of systems. Nucl. Phys. A **764**, 135–148 (2006). https://doi.org/10.1016/j.nuclphysa.2005.09.001
37. D. Carbone, J.L. Ferreira, F. Cappuzzello et al., Microscopic cluster model for the description of new experimental results on the ^{13}C(^{18}O,^{16} O)^{15}C two-neutron transfer at 84 MeV incident energy. Phys. Rev. C **95**, 034603 (2017). https://doi.org/10.1103/PhysRevC.95.034603
38. C. Qi, R. Liotta, R. Wyss, Recent developments in radioactive charged-particle emissions and related phenomena. Prog. Part. Nucl. Phys. **105**, 214–251 (2019). https://doi.org/10.1016/j.ppnp.2018.11.003
39. W. Horiuchi, N. Itagaki, Imprints of α clustering in the density profiles of ^{12}C and ^{16}O. Phys. Rev. C. **107**, L021304 (2023). https://doi.org/10.1103/PhysRevC.107.L02130
40. C. Bloch, J.L. Gammel, Many-body description of nuclear structure and reactions. Phys. Today **21**, 103–105 (1968). https://doi.org/10.1063/1.3034946
41. E. Uegaki, S. Okabe, Y. Abe et al., Structure of the excited states in ^{12}C. Prog. Theor. Phys. **57**, 1262–1276 (1977). https://doi.org/10.1143/PTP.57.1262

42. C. Ishizuka, H. Takemoto, Y. Chiba et al., Role of tensor interaction as salvation of cluster structure in ^{44}Ti. Phys. Rev. C. **105**, 064314 (2022). https://doi.org/10.1103/PhysRevC.105.064314
43. M. Kamimura, Transition densities between the 0_1^+, 2_1^+, 4_1^+, 0_2^+, 2_2^+, 1_1^- and 3_1^- states in ^{12}C derived from the three-alpha resonating-group wave functions. Nucl. Phys. A. **351**, 456–480 (1981). https://doi.org/10.1016/0375-9474(81)90182-2
44. P. Descouvemont, ^{12}C (α,γ) ^{16}O E2 cross section in a microscopic four-alpha model. Phys. Rev. C. **47**, 210 (1993). https://doi.org/10.1103/PhysRevC.47.210
45. N. Itagaki, A. Ohnishi, K. Katō, Microscopic α-cluster model for ^{12}C and ^{16}O based on antisymmetrized molecular dynamics: Consistent understanding of the binding energies of ^{12}C and ^{16}O. Prog. Theor. Phys. **94**, 1019–1038 (1995). https://doi.org/10.1143/PTP.94.1019
46. A. Tohsaki, H. Horiuchi, P. Schuck et al., Alpha cluster condensation in ^{12}C and ^{16}O. Phys. Rev. Lett. **87**, 192501 (2001). https://doi.org/10.1103/PhysRevLett.87.192501
47. T. Otsuka, T. Abe, T. Yoshida et al., α-clustering in atomic nuclei from first principles with statistical learning and the Hoyle state character. Nat. Commun. **13**, 2234 (2022). https://doi.org/10.1038/s41467-022-29582-0
48. Y. Kanada-En'yo, The structure of ground and excited states of ^{12}C. Prog. Theor. Phys. **117**, 655–680 (2007). https://doi.org/10.1143/PTP.117.655
49. M. Chernykh, H. Feldmeier, T. Neff et al., Structure of the Hoyle state in ^{12}C. Phys. Rev. Lett. **98**, 032501 (2007). https://doi.org/10.1103/PhysRevLett.98.032501
50. J.L. Ferreira, J. Lubian, R. Linares et al., Analysis of the alpha-transfer reaction in the $^{12}\mathrm{C}+{}^{16}\mathrm{O}$ system using the semi-microscopic algebraic cluster model. Eur. Phys. J. A. **55**, 94 (2019). https://doi.org/10.1140/epja/i2019-12773-7
51. G.R. Satchler, *Direct Nuclear Reactions* (Oxford University Press, Oxford, 1983)
52. M. Moshinsky, Transformation brackets for harmonic oscillator functions. Nucl. Phys. **13**, 104–116 (1959). https://doi.org/10.1016/0029-5582(59)90143-9
53. W.D.M. Rae, http://www.garsington.eclipse.co.uk/
54. B.A. Brown, N.J. Stone, J.R. Stone et al., Magnetic moments of the 2_1^+ states around ^{132}Sn. Phys. Rev. C **71**, 044317 (2005). https://doi.org/10.1103/PhysRevC.71.044317
55. R. Machleidt, The meson theory of nuclear forces and nuclear structure. Adv. Nucl. Phys. 189–376 (1989)
56. R. Machleidt, High-precision, charge-dependent Bonn nucleon–nucleon potential. Phys. Rev. C **63**, 024001 (2001). https://doi.org/10.1103/PhysRevC.63.024001
57. H. Mach, E.K. Warburton, R.L. Gill et al., Meson-exchange enhancement of the first-forbidden $^{96}\mathrm{Y}^{\mathrm{g}}(0^-)\rightarrow{}^{96}\mathrm{Zr}^{\mathrm{g}}(0^+)$ β transition : β decay of the low − spin isomer of ^{96}Y. Phys. Rev. C **41**, 226–242 (1990). https://doi.org/10.1103/PhysRevC.41.226
58. S.P. Hu, G.L. Zhang, J.C. Yang et al., One-neutron stripping processes to excited states of the $^{6}\mathrm{Li}+{}^{96}\mathrm{Zr}$ reaction at near-barrier energies. Phys. Rev. C **93**, 014621 (2016). https://doi.org/10.1103/PhysRevC.93.014621
59. E. Warburton, A. Brown, Effective interactions for the 0p1s0d nuclear shell-model space. Phys. Rev. C **46**, 923 (1992). https://doi.org/10.1103/PhysRevC.46.923
60. D.M. Brink, Kinematical effects in heavy-ion reactions. Phys. Lett. B **40**, 37–40 (1972). https://doi.org/10.1016/0370-2693(72)90274-2
61. J.C. Zamora, J.L. Ferreira, A. Barioni et al., Role of direct mechanism in two-nucleon $t=0$ transfer reactions in light nuclei using the $(^{6}\mathrm{Li},\alpha)$ probe. Phys. Rev. C **106**, 014603 (2022). https://doi.org/10.1103/PhysRevC.106.014603